

Golden Noise for Diffusion Models: A Learning Framework

Zikai Zhou¹, Shitong Shao¹, Lichen Bai¹, Shufei Zhang², Zhiqiang Xu³, Bo Han⁴, Zeke Xie^{1*}
¹ HKUST-GZ ² Shanghai AI Lab ³ MBZUAI ⁴ HKBU

{zikaizhou, sshao213, lichenbai, zekexie}@hkust-gz.edu.cn

zhangshufei@pjlab.org.cn zhiqiang.xu@mbzuai.ac.ae bhanml@comp.hkbu.edu.hk

Github: <https://github.com/xie-lab-ml/Golden-Noise-for-Diffusion-Models>

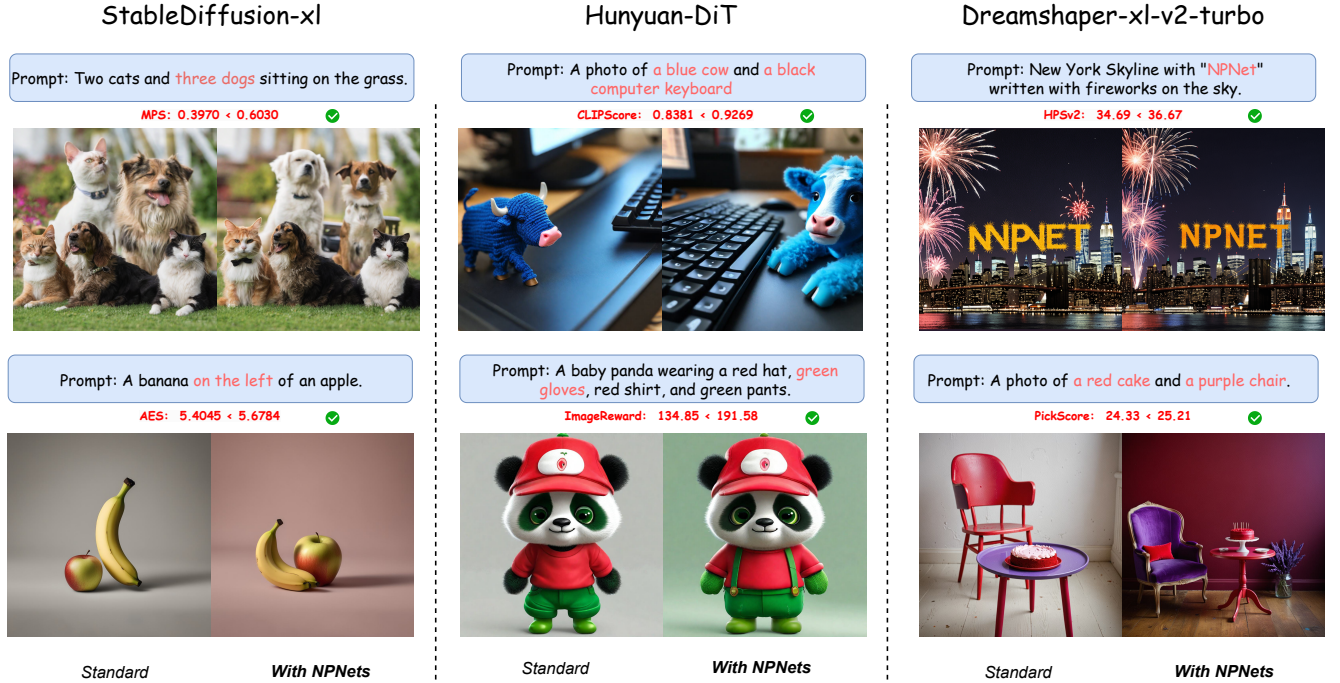


Figure 1. We visualize images synthesized by 3 different diffusion models and evaluate them using 6 human preference metrics. Images for each prompt are synthesized using the same random seed. These images with NPNet demonstrate a noticeable improvement in overall quality, aesthetic style, and semantic faithfulness, along with numerical improvements across all six metrics. More importantly, our NPNet is applicable to various diffusion models, showcasing strong generalization performance with broad application potential. More visualization results are in Appendix 22.

Abstract

Text-to-image diffusion model is a popular paradigm that synthesizes personalized images by providing a text prompt and a random Gaussian noise. While people observe that some noises are “golden noises” that can achieve better text-image alignment and higher human preference than others, we still lack a machine learning framework to obtain those golden noises. To learn golden noises for diffusion sampling, we mainly make three contributions in this paper. First, we identify a new concept termed the noise prompt, which aims at turning a random Gaussian noise

into a golden noise by adding a small desirable perturbation derived from the text prompt. Following the concept, we first formulate the noise prompt learning framework that systematically learns “prompted” golden noise associated with a text prompt for diffusion models. Second, we design a noise prompt data collection pipeline and collect a large-scale noise prompt dataset (NPD) that contains 100k pairs of random noises and golden noises with the associated text prompts. With the prepared NPD as the training dataset, we trained a small noise prompt network (NPNet) that can directly learn to transform a random noise into a golden noise. The learned golden noise perturbation can be con-

sidered as a kind of prompt for noise, as it is rich in semantic information and tailored to the given text prompt. Third, our extensive experiments demonstrate the impressive effectiveness and generalization of NPNet on improving the quality of synthesized images across various diffusion models, including SDXL, DreamShaper-xl-v2-turbo, and Hunyuan-DiT. Moreover, NPNet is a small and efficient controller that acts as a plug-and-play module with very limited additional inference and computational costs, as it just provides a golden noise instead of a random noise without accessing the original pipeline.

1. Introduction

Image synthesis that are precisely aligned with given text prompts remains a significant challenge for text-to-image (T2I) diffusion models [4, 7, 35, 36, 42]. Previous studies [24, 28, 50, 52, 57] have investigated the influence of text embeddings on the synthesized images and leveraged these embeddings for training-free image synthesis. It is well known that text prompts significantly matter to the quality and fidelity of the synthesized images. However, image synthesis is induced by both the text prompts and the noise. Variations in the noise can lead to substantial changes in the synthesized images, as even minor alterations in the noise input can dramatically influence the output [38, 56]. This sensitivity underscores the critical role that noise plays in shaping the final visual representation, affecting both the overall aesthetics and the semantic faithfulness between the synthesized images and the provided text prompt.

Recent studies [2, 5, 8, 11, 32, 38] observe that some selected or optimized noises are golden noises that can help the T2I diffusion models to produce images of better semantic faithfulness with text prompts, and can also improve the overall quality of the synthesized images. These methods [5, 11] incorporate extra modules like attention to reduce the truncate errors during the sampling process, showing promising results on the compositional generalization task. However, they are often not widely adopted in practice for several reasons. First, they often struggle to generally transfer to various benchmark datasets or diffusion models but only work for some specific tasks. Second, these methods often introduce significant time delays in order to optimize the noises during the reverse process. Third, they require in-depth modifications to the original pipelines when applied to different T2I diffusion models with varying architectures. Fourth, they need specific subject tokens for each prompt to calculate the loss of certain areas, which are unrealistic requirements for real users. These not only significantly complicate the original inference pipeline but also raise concerns regarding the generalization ability across various T2I diffusion models and datasets.

In light of the aforementioned research, we pose sev-

eral critical questions: 1) Can we formulate obtaining the golden noises as a machine learning problem so that we can predict them efficiently with only one model forward inference? 2) Can such a machine learning framework generalize well to various noises, prompts, and even diffusion models? Fortunately, the answers are affirmative. In this paper, we mainly make three contributions:

First, we identify a new concept termed *noise prompt*, which aims at turning a random noise into a golden noise by adding a small desirable perturbation derived from the text prompt. The golden noise perturbation can be considered as a kind of prompt for noise, as it is rich in semantic information and tailored to the given text prompt. Building upon this concept, we formulate a *noise prompt learning* framework that learns “prompted” golden noises associated with text prompts for diffusion models.

Second, to implement the formulated *noise prompt learning* framework, we propose the training dataset, namely the *noise prompt dataset* (NPD), and the learning model, namely the *noise prompt network* (NPNet). Specifically, we design a noise prompt data collection pipeline via *re-denoise sampling*, a way to produce noise pairs. We also incorporate AI-driven feedback mechanisms to ensure that the noise pairs are highly valuable. This pipeline enables us to collect a large-scale training dataset for noise prompt learning, so the trained NPNet can directly transform a random Gaussian noise into a golden noise to boost the performance of the T2I diffusion model.

Third, we conduct extensive experiments across various mainstream diffusion models, including StableDiffusion-xl (SDXL) [37], DreamShaper-xl-v2-turbo and Hunyuan-DiT [25], with 7 different samplers on 4 different datasets. We evaluate our model by utilizing 6 human preference metrics including Human Preference Score v2 (HPSv2) [53], PickScore [23], Aesthetic Score (AES) [46], ImageReward [55], CLIPScore [12] and Multi-dimensional Preference Score (MPS) [59]. As illustrated in Fig. 1, by leveraging the learned golden noises, not only is the overall quality and aesthetic style of the synthesized images visually enhanced, but all metrics also show significant improvements, demonstrating the effectiveness and generalization ability of our NPNet. Furthermore, the NPNet is a compact and efficient neural network that functions as a plug-and-play module, introducing only a **3%** extra inference time per image compared to the standard pipeline, while requiring approximately 3% of the memory required by the standard pipeline. This underscores the practical applicability of NPNet in real-world scenarios.

2. Preliminaries

We first present preliminaries about DDIM and DDIM Inversion and the classifier-free guidance. Due to the space constraints, we introduce the related work in Appendix B.

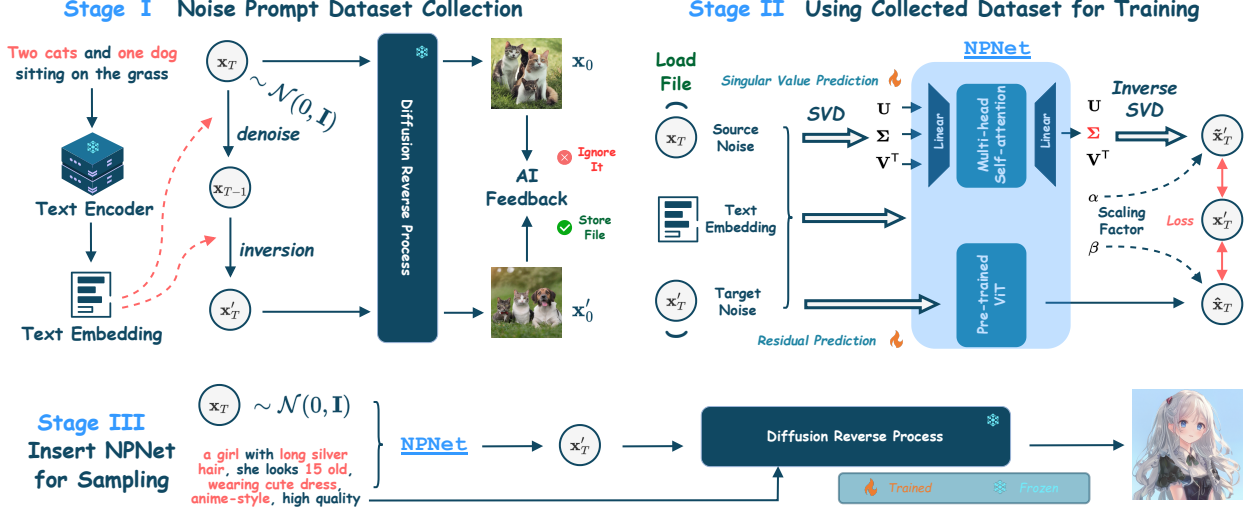


Figure 2. Our workflow diagram consists of three main stages. *Stage I*: We begin by denoising the original random Gaussian noise \mathbf{x}_T to obtain \mathbf{x}_{T-1} , and then use DDIM-Inversion(\cdot) to obtain inverse \mathbf{x}'_T with more semantic information. Both synthesized images \mathbf{x}_0 and \mathbf{x}'_0 are filtered by the human preference model, such as HPSv2, to ensure the dataset is both diverse and representative. *Stage II*: After collecting NPD, we input the original noise (source noise) \mathbf{x}_T , inverse noise (target noise) \mathbf{x}'_T and text prompt \mathbf{c} into the NPNNet, where the noises are processed by the *singular value predictor* and the *residual predictor*, and text prompt \mathbf{c} is encoded by the text encoder $\mathcal{E}(\cdot)$ of the T2I diffusion model, resulting in the golden noise. *Stage III*: Once trained, our NPNNet can directly convert the random Gaussian noise into a golden noise before inputting T2I diffusion models, boosting the performance of these models.

Given the Gaussian noise $\epsilon_t \sim \mathcal{N}(0, \mathbf{I})$, we denote the forward process of diffusion models as $\mathbf{x}_t = \alpha_t \mathbf{x}_0 + \sigma_t \epsilon_t$, where the $t \in \{0, 1, \dots, T\}$. Here, α_t and σ_t are predefined noise schedules, and \mathbf{x}_0 is the original image.

DDIM and DDIM Inversion. Denoising diffusion implicit model (DDIM) [48] is an advanced deterministic sampling technique, deriving an implicit non-Markov sampling process of the diffusion model. It allows for faster synthesis while maintaining the quality of synthesized samples. Its reverse process can be formulated as:

$$\begin{aligned} \mathbf{x}_{t-1} &= \text{DDIM}(\mathbf{x}_t) \\ &= \alpha_{t-1} \left(\frac{\mathbf{x}_t - \sigma_t \epsilon_\theta(\mathbf{x}_t, t)}{\alpha_t} \right) + \sigma_{t-1} \epsilon_\theta(\mathbf{x}_t, t) \end{aligned} \quad (1)$$

Using DDIM to add noise is called DDIM-Inversion:

$$\begin{aligned} \mathbf{x}_t &= \text{DDIM-Inversion}(\mathbf{x}_{t-1}) \\ &= \frac{\alpha_t}{\alpha_{t-1}} \mathbf{x}_{t-1} + \left(\sigma_t - \frac{\alpha_t}{\alpha_{t-1}} \sigma_{t-1} \right) \epsilon_\theta(\mathbf{x}_t, t) \end{aligned} \quad (2)$$

Classifier-free Guidance (CFG). Classifier-free guidance [14] allows for better control over the synthesis process by guiding the diffusion model towards desired conditions, such as text prompt, to enhance the quality and diversity of synthesized samples. The predicted noise ϵ_{pred} with CFG at timestep t can be formulated as:

$$\epsilon_{pred} = (\omega + 1) \epsilon_\theta(\mathbf{x}_t, t | \mathbf{c}) - \omega \epsilon_\theta(\mathbf{x}_t, t | \emptyset), \quad (3)$$

where we denote the \mathbf{c} as the text prompt, ω as the CFG scale. Based on this, the denoised image \mathbf{x}_{t-1} by using DDIM(\cdot) can be written as:

$$\begin{aligned} \mathbf{x}_{t-1} &= \alpha_{t-1} \left(\frac{\mathbf{x}_t - \sigma_t [(\omega + 1) \epsilon_\theta(\mathbf{x}_t, t | \mathbf{c}) - \omega \epsilon_\theta(\mathbf{x}_t, t | \emptyset)]}{\alpha_t} \right) \\ &\quad + \sigma_{t-1} [(\omega + 1) \epsilon_\theta(\mathbf{x}_t, t | \mathbf{c}) - \omega \epsilon_\theta(\mathbf{x}_t, t | \emptyset)] \end{aligned} \quad (4)$$

3. Noise Prompt Learning

In this section, we present the methodology of noise prompt learning, including NPD collection, NPNNet design and training, as well as sampling with NPNNet.

Noise prompt can be considered as a kind of special prompt, which aims at turning a random noise into a golden noise by adding a small desirable perturbation derived from the text prompt. Analogous to text prompts, appropriate noise prompts can enable diffusion models to synthesize higher-quality images that are rich in semantic information. As illustrated on the left in Appendix Fig. 6, *text prompt learning* in large language models [30] focuses on learning how to transform a text prompt into a more desirable version. Similarly, *noise prompt learning* in our work seeks to learn how to convert the random Gaussian noise into the golden noise by adding a small, desirable perturbation derived from the text prompt. Using the golden noise, the diffusion model can synthesize images with higher quality and semantic faithfulness. Defining it as a machine learning problem, we are the first to formulate the *noise prompt learning* framework, as illustrated on the right in Appendix

Fig. 6. Given the training set $\mathcal{D} := \{\mathbf{x}_{T_i}, \mathbf{x}'_{T_i}, \mathbf{c}_i\}_{i=1}^{|\mathcal{D}|}$ consisting of source noises \mathcal{X} , target noises \mathcal{X}' and text prompts \mathcal{C} , loss function ℓ and the neural network ϕ , the general formula for the *noise prompt learning* task is:

$$\phi^* = \arg \min_{\phi} \mathbb{E}_{(\mathbf{x}_{T_i}, \mathbf{x}'_{T_i}, \mathbf{c}_i) \sim \mathcal{D}} [\ell(\phi(\mathbf{x}_{T_i}, \mathbf{c}_i), \mathbf{x}'_{T_i})]. \quad (5)$$

In summary, our goal is to learn the optimal neural network model ϕ^* trained on the training set \mathcal{D} . We present the data-training-inference workflow diagram with three stages in Appendix Fig. 6 and provide the pseudocodes for each stage in Appendix Alg. 1, Alg. 2 and Alg. 3, respectively.

3.1. Noise Prompt Dataset Collection

In this subsection, we outline the training data collection pipeline, which consists of collecting noise pairs and AI-feedback-based data selection, as shown in Fig. 2 Stage I.

Re-denoise Sampling Produces Noise Pairs. *How to collect noises with desirable semantic information?* Meng et al. [34] reported that adding the random noise at each timestep during the sampling process and then re-denoising, leads to a substantial improvement in the semantic faithfulness of the synthesized images. This motivated us to propose a simple and direct approach called RE-DENOISE SAMPLING. Instead of directly adding noise to each timestep during the reverse process, we propose to utilize DDIM-Inversion(\cdot) to obtain the noise from the previous step. Specifically, the joint action of DDIM-Inversion and CFG can induce the initial noise to attach semantic information. We denote the CFG scale within DDIM(\cdot) and DDIM-Inversion(\cdot) as ω_l and ω_w , respectively. It is sufficient to ensure that the initial noise can be purified stably and efficiently by $\mathbf{x}'_t = \text{DDIM-Inversion}(\text{DDIM}(\mathbf{x}_t))$ with $\omega_l > \omega_w$. Utilizing this method, the synthesized image from \mathbf{x}'_t is more semantic information contained with higher fidelity, compared with the synthesized image from \mathbf{x}_t . We call the inverse noise \mathbf{x}'_t target noise, and the noise \mathbf{x}_t source noise. The visualization results are shown in Appendix Fig. 7 and 9. The mechanism behind this method is that DDIM-Inversion(\cdot) injects semantic information by leveraging the CFG scale inconsistency. We present **theoretical understanding** of this mechanism in Theorem E.1.

Data Selection with the Human Preference Model.

While employing *re-denoise sampling* can help us collect noises with enhanced semantic information, it also carries the risk of introducing extra noises, which may lead to synthesizing images that do not achieve the quality of the originals. To mitigate this issue, we utilize a human preference model for data selection. This model assesses the synthesized images based on human preferences, allowing us to retain those noise samples that meet our quality standards.

The reservation probability for data selection can be formulated as $\mathbb{I}[s_0 + m < s'_0]$, where m is the filtering threshold, $\mathbb{I}[\cdot]$, s_0 and s'_0 are the indicator function, human preference scores of denoised images from \mathbf{x}_0 and \mathbf{x}'_0 , respectively. If the noise samples meet this criterion, we consider them to be valuable noise pairs and proceed to collect them.

By implementing this filtering process, we aim to balance the benefits of *re-denoise sampling* with the integrity of the synthesized outputs. For the selection strategies, we introduce them in Appendix Sec. D.2.

3.2. Noise Prompt Network

Here, we introduce the architecture, training, inference of NPNet, as shown in Fig. 2 Stage II and Stage III.

Architecture Design. The architecture of NPNet consists of two key components, including *singular value prediction* and *residual prediction*, as shown in Fig. 2 Stage II.

The first key model component is *singular value prediction*. We obtain noise pairs through *re-denoise sampling*, a process that can be approximated as adding a small perturbation to the source noises. We observe that through the *singular value decomposition* (SVD), the singular vectors of \mathbf{x}_T and \mathbf{x}'_T exhibit remarkable similarity, albeit possibly in opposite directions, shown in Appendix Fig. 8, which may be partly explained by Davis-Kahan Theorem [49, 54]. Building upon this observation, we design an architecture to predict the singular values of the target noise, illustrated in Fig. 2 Stage II. We denote $\phi(\cdot, \cdot, \cdot)$ as a ternary function that represents the sum of three inputs, $f(\cdot)$ as the linear layer function, and $g(\cdot)$ as the multi-head self-attention layer. The paradigm can be formulated as:

$$\begin{aligned} \mathbf{x}_T &= U \times \Sigma \times V^T, & \tilde{\mathbf{x}}_T &= \phi(U, \Sigma, V^T), \\ \tilde{\Sigma} &= f(g(\tilde{\mathbf{x}}_T)), & \tilde{\mathbf{x}}'_T &= U \times \tilde{\Sigma} \times V^T, \end{aligned} \quad (6)$$

where we denote $\tilde{\mathbf{x}}'_T$ as the predicted target noise. This model utilizes SVD inverse transformation to effectively reconstruct the target noise. By leveraging the similarities in the singular vectors, our model enhances the precision of the target noise restoration process.

The second key model component is residual prediction. In addition to *singular value prediction*, we also design an architecture to predict the residual between the source noise and the target noise, as illustrated in Fig. 2 Stage II. We denote $\varphi(\cdot)$ as the UpSample-DownConv operation, $\varphi'(\cdot)$ as the DownSample-UpConv operation, and the $\psi(\cdot)$ as the ViT model. The target noise incorporates semantic information from the text prompt \mathbf{c} introduced through CFG. To facilitate the learning process, we inject this semantic information using the frozen text encoder $\mathcal{E}(\cdot)$ of the T2I diffusion model. This approach allows the model to effectively leverage the semantic information provided by the

Table 1. Summary of the experiments in this paper.

Experiments		Results
Main Experiments		Table 2, 3, Appendix Table 8 and 13 Fig. 3, Appendix Fig. 12, 14 and 17
Generalization	Various Datasets and Models	Table 2, 3, Appendix Table 6, 19 and 18 Fig. 3
	Stochastic/Deterministic Samplers	Appendix Table 11 Fig. 5 and Appendix Fig. 10
	Orthogonal Experiment	Table 5, Appendix Table 20 and Fig. 19
Robustness to Hyper-parameters		Appendix Table 12 and 17 Fig. 4, Appendix Fig. 14, 16 and 17
Ablation Studies		Table 4, Appendix Table 9 and 10
Efficiency		Appendix Table 11 Fig. 5 and Appendix Fig. 10
Downstream Task		Appendix Fig. 20
Visualization		Fig. 1, Appendix Fig. 20, 22, 24, 25, 26, 27, 28, 29, 31, 30, 32 and 33.

text prompt, ultimately improving the accuracy of the residual prediction. The procedure can be described as follows:

$$\mathbf{e} = \sigma(\mathbf{x}_T, \mathcal{E}(\mathbf{c})) \quad \hat{\mathbf{x}}_T = \varphi'(\psi(\varphi(\mathbf{x}_T + \mathbf{e}))), \quad (7)$$

where we denote $\sigma(\cdot, \cdot)$ as AdaGroupNorm to stabilize the training process, and \mathbf{e} as the normalized text embedding.

Using Collected Dataset for Training. The training procedure is also illustrated in Fig. 2 *Stage II*. To yield optimal results, we formulate the training loss as

$$\begin{aligned} \mathcal{L}_{\text{MSE}} &= \text{MSE}(\mathbf{x}'_T, \mathbf{x}'_{T_{\text{pred}}}), \\ \text{where } \mathbf{x}'_{T_{\text{pred}}} &= \tilde{\mathbf{x}}_T + \beta \hat{\mathbf{x}}_T, \end{aligned} \quad (8)$$

β is a trainable parameter used to adaptively adjust the weights of the predicted residuals, and L as the $\text{MSE}(\cdot)$ loss function. For the nuanced adjustment in how much semantic information contributes to the model’s predictions, $\mathbf{x}'_{T_{\text{pred}}} = \tilde{\mathbf{x}}_T + \beta \hat{\mathbf{x}}_T$ can be rewritten as:

$$\mathbf{x}'_{T_{\text{pred}}} = \alpha \mathbf{e} + \tilde{\mathbf{x}}_T + \beta \hat{\mathbf{x}}_T, \quad (9)$$

where we denote α as a trainable parameter. The values of these two parameters are shown in Appendix Table 15. We notice that α is very small, but it still plays a role in adjusting the influence of injected semantic information (see Appendix Table 16 for experimental results). Together, α and β finely control the impact of semantic information on the model’s predictions, enhancing both the semantic relevance between the text prompt and synthesized images and the diversity of these images.

Insert NPNet for Sampling. The inference procedure is illustrated in Fig. 2 *Stage III*. Once trained, our NPNet can be directly applied to the T2I diffusion model by inputting the initial noise \mathbf{x}_T and prompt embedding \mathbf{c} encoded by the frozen text encoder of the diffusion model. Our NPNet

can effectively transform the original initial noise into the golden noise. We also provide the example code on SDXL, shown in the Appendix Fig. 21.

4. Empirical Analysis

In this section, we empirically study the effectiveness, the generalization, and the efficiency of our NPNet. We conduct a lot of experiments across various datasets on various T2I diffusion models, including SDXL, DreamShaper-xl-v2-turbo, and Hunyuan-DiT. Due to space constraints, we leave implementation details, related work and additional experiments in Appendix A, C and D, respectively. We also leave the discussion and future direction in Appendix F. To assist readers in better understanding this paper, we have summarized the main tables and figures in Table. 1.

Description of Training and Test Data. We collect our NPD on Pick-a-pic dataset [23], which contains 1M prompts in its training set. We randomly choose 100k prompts as our training set. For each prompt, we randomly assign a seed value in $[0, 1024]$. For testing, we use three datasets, including the first 100 prompts from the Pick-a-Pic web application, the first 100 prompts from HPD v2 test set [53], all 200 prompts from DrawBench [45], all prompts from GenEval [10] and T2I-CompBench [20]. For more details about the test data, please see Appendix Fig. 18. We construct three training datasets collected from Pick-a-Pic, with 100k noise pairs, 80k noise pairs, and 600 noise pairs for SDXL, DreamShaper-xl-v2-turbo, and Hunyuan-DiT.

4.1. Main Results

We evaluate our NPNet in three different T2I diffusion models. The main results¹ are shown in Table 2 and Table 3. In Table 2, we first evaluate our NPNet with SDXL and DreamShaper-xl-v2-turbo. The results demonstrate the impressive performance of our NPNet, almost achieving the

¹Method “Inversion” means *re-denoise sampling*.

Table 2. Main experiments on SDXL and DreamShaper-xl-v2-turbo over various datasets. Note that MPS calculates the preference scores between two images. We choose the standard sampling as the baseline and the MPS score is always 50%, marked as “—”.

Model	Dataset	Method	PickScore (↑)	HPSv2 (↑)	AES (↑)	ImageReward (↑)	CLIPScore (↑)	MPS(%) (↑)
SDXL	Pick-a-Pic	Standard	21.69	28.48	6.0373	58.01	0.8204	-
		Inversion ¹	21.71	28.57	6.0503	63.27	0.8250	51.41
		NPNNet (ours)	21.86	28.68	6.0540	65.01	0.8408	52.14
	DrawBench	Standard	22.31	26.72	5.5952	62.21	0.8077	-
		Inversion	22.37	26.91	5.6017	67.09	0.8081	51.98
		NPNNet (ours)	22.38	27.14	5.6034	70.67	0.8153	53.70
	HPD	Standard	22.88	29.71	5.9985	96.63	0.8734	-
		Inversion	22.89	29.78	5.9948	97.39	0.8708	53.03
		NPNNet (ours)	22.94	29.88	5.9922	98.81	0.8813	56.02
DreamShaper-xl-v2-turbo	Pick-a-Pic	Standard	22.41	32.12	6.0161	98.09	0.8267	-
		Inversion	22.40	32.03	6.0236	100.97	0.8277	49.14
		NPNNet (ours)	22.73	32.69	6.0646	106.74	0.8958	52.34
	DrawBench	Standard	22.98	30.39	5.6735	98.84	0.8186	-
		Inversion	22.94	30.10	5.6852	96.74	0.8189	46.62
		NPNNet (ours)	23.11	30.78	5.7005	108.14	0.8224	53.53
	HPD	Standard	23.68	30.96	6.1408	129.89	0.8868	-
		Inversion	23.67	31.00	6.0811	131.80	0.8912	46.94
		NPNNet (ours)	23.70	34.08	6.1283	135.98	0.8942	52.49

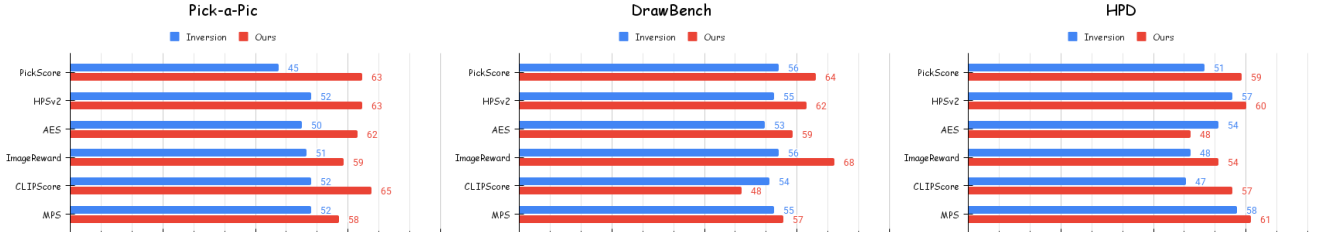


Figure 3. The winning rate comparison on SDXL across 3 datasets, including Pick-a-Pic, DrawBench and HPD v2 (HPD). The results reveal that our NPNNet is the only one that can consistently transform random Gaussian noise into golden noises, thereby enhancing the quality of the synthesized images, across nearly all evaluated datasets and metrics.

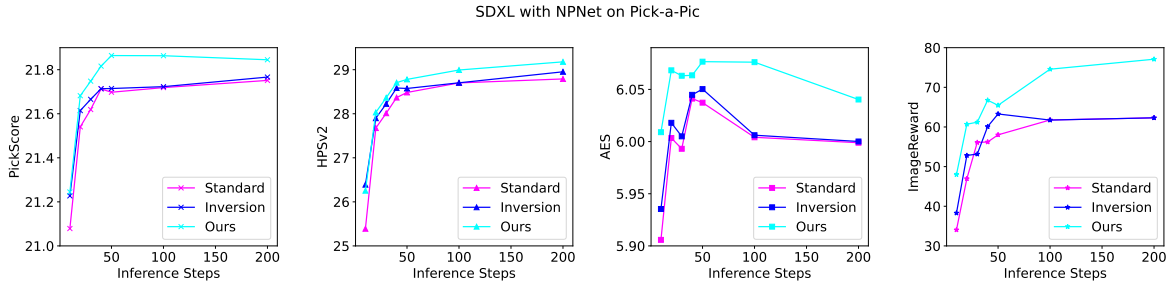


Figure 4. Visualization of performance w.r.t. inference steps on SDXL on Pick-a-Pic dataset. With our NPNNet, T2I diffusion models can have superior performance under various inference steps.

Table 3. The fine-tuned NPNNet showing strong cross-model generalization to enhancing Hunyuan-DiT, requiring only Hunyuan-DiT-produced 600 noise pairs for fine-tuning.

Dataset	Method	PickScore (↑)	HPSv2 (↑)	AES (↑)	ImageReward (↑)	CLIPScore(%) (↑)	MPS(%) (↑)
Pick-a-Pic	Standard	21.82	29.82	6.2850	91.33	80.37	-
	Inversion	21.76	29.64	6.2756	88.77	80.21	49.08
	NPNNet (ours)	21.84	29.94	6.3470	100.82	81.01	51.60
DrawBench	Standard	22.44	28.75	5.7152	91.30	79.40	-
	Inversion	22.44	28.75	5.7522	92.86	79.55	49.25
	NPNNet (ours)	22.45	28.89	5.8234	96.20	80.75	51.93
HPD	Standard	22.89	30.87	6.0793	99.22	85.68	-
	Inversion	22.90	30.56	6.0802	100.21	86.17	51.63
	NPNNet (ours)	22.89	31.20	6.1573	108.29	86.94	52.87

best results across all 6 metrics and 3 datasets. Due to the space limitations, we present the experiments on GenEval and T2I-CompBench in Appendix D.7 and 8. We also evaluate our fine-tuned NPNet with Hunyuan-DiT, as shown in Table 3. For Hunyuan-DiT, we directly utilized the NPNet model trained on SDXL-produced NPD and fine-tune it on the Hunyuan-DiT-produced 600 noise pairs. Fine-tuned with only 600 samples, it can still achieve the highest results over the baselines on Hunyuan-DiT. This highlights the strong cross-model generalizability of our NPNet.

We also show the winning rate (the ratio of winning noise in the test set) on SDXL with our NPNet, shown in Fig. 3. We present more winning rate experiments of DreamShaper-xl-v2-turbo and Hunyuan-DiT in Appendix Fig. 14 and Appendix Fig. 17. These results again support that our NPNet is highly effective in transforming random Gaussian noise into golden noises. In order to validate the effectiveness of our NPNet on improving the conventional image quality metric, we also calculate the FID [13] of 5000 images on class conditional ImageNet with resolution 512×512 (please see more implementation details in Appendix D), shown in Appendix Fig. 12. We present more visualization results in Appendix Fig. 23.

We further study samples synthesized with and without NPNet to assess the distribution shift. Our empirical analysis reveals that NPNet effectively mitigates distributional discrepancies, resulting in synthesized images that exhibit statistically significant alignment with the true data manifold, shown in Appendix Fig. 13.

Table 4. Ablation studies of the proposed methods on SDXL.

Method	PickScore (↑)	HPSv2 (↑)	AES (↑)	ImageReward (↑)
Standard	21.69	28.48	6.0373	58.01
NPNet w/o singular value prediction	21.49	27.76	6.0164	49.03
NPNet w/o residual prediction	21.83	28.55	6.0315	63.05
NPNet w/o data selection	21.73	28.46	6.0375	62.91
NPNet	21.86	28.68	6.0540	65.01

4.2. Analysis of Generalization and Robustness

To validate the superior generalization ability of our NPNet, we conduct multiple experiments, covering experiments of cross-dataset, cross-model architecture, various inference steps, various random seed ranges, stochastic/deterministic samplers, and the integration of other methods.

Generalization to Various Datasets and Models. Although we trained our NPNet exclusively with the NPDs collected from the Pick-a-Pic dataset, the experimental results presented in Table 2 and Table 3, and Fig. 3 demonstrate that our model exhibits strong cross-dataset generalization capabilities, achieving impressive results on other datasets as well. In addition to the fine-tuning experiments detailed in Table 3, we also applied the NPNet trained on NPD collected from SDXL to DreamShaper-xl-v2-turbo, evaluating the performance with our NPNet without any

fine-tuning. The experiment results are shown in Appendix Table 6. Moreover, We use the same NPNet from SDXL and apply it directly on few steps T2I diffusion model, such as LCM [33], PCM [51] and SDXL-Lightning [26], which also improves the quality of the synthesized images, shown in Appendix Table 18. These results indicate promising performance with our NPNet, underscoring the model’s capability for cross-model generalization. We also conduct experiments on noise seed range in Appendix Table 19, the results demonstrate that our NPNet exhibits strong generalization capabilities across the out-of-distribution random seed ranges without harming the image diversity.

Generalization to Stochastic/Deterministic Samplers.

When collecting NPD on SDXL, we use the deterministic DDIM sampler. However, whether the NPNet can effectively perform with stochastic samplers is crucial. To investigate our NPNet’s performance across various sampling methods, we evaluated 7 different samplers, using NPNet trained on the NPD collected from SDXL, whose sampler is DDIM. The results shown in Fig. 5 and Appendix Table 11 suggest that our NPNet is adaptable and capable of maintaining high performance even when subjected to various levels of randomness in the sampling process, further validating the generalization of our NPNet.

Table 5. We conducted combinatorial experiments with other mainstream methods that can improve the alignment between the text prompts and synthesized images. The results indicate that our approach is orthogonal to these methods, allowing for joint usage to achieve improved performance.

Methods	PickScore (↑)	HPSv2 (↑)	AES (↑)	ImageReward (↑)
Standard	21.07	25.38	5.9058	34.04
DPO	21.83	28.42	5.9993	68.82
DPO+NPNet (ours)	21.91	28.70	6.0277	75.06
Standard	21.07	25.38	5.9058	34.04
AYS	21.53	27.24	6.0310	50.74
AYS+NPNet (ours)	21.76	28.14	6.1239	59.50

Orthogonal Experiment. To explore whether our model can be combined with other approaches, which aim at enhancing the semantic faithfulness of synthesized images, such as DPO [40] and AYS [43], we conduct combination experiments, shown in Table 5. Note that AYS only releases the code under the inference step 10, so we conduct the combinatorial experiment with AYS and DPO (for consistency) under the inference step 10. The results indicate that our method is orthogonal to these works, allowing for joint usage to further improve the quality of synthesized images.

More notably, we significantly improve the performance and winning rate of the previous noise optimization methods by using NPNet together with them, which further illustrates the effectiveness and scalability of our NPNet, shown in Appendix Table 20 and Fig. 19.

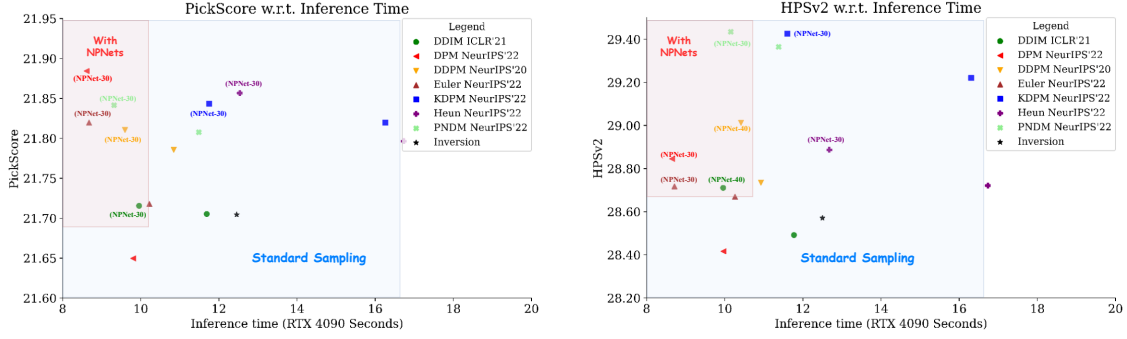


Figure 5. We evaluate our NPNet with 7 samplers on SDXL in Pick-a-Pic dataset, including both the deterministic sampler and stochastic sampler (with a default inference step 50). “NPNet-30” means the inference step is 30 with NPNet. The red area in the top left corner of the image represents the results of efficient high-performance methods, while the experimental results of NPNet are nearly in that same region. It highlights that NPNet is capable of synthesizing higher-quality images with fewer steps and consuming less time. Moreover, the results demonstrate the generalization ability of our NPNet across different samplers.

Robustness to the Hyper-parameters. We study how the performance of NPNet is robust to the hyper-parameters. We first evaluate the performance of our NPNet under various inference steps, as illustrated in Fig. 4, Appendix Fig. 14, Appendix Fig. 16, and Appendix Fig. 17. These results highlight the generalization and versatility of our NPNet is robust to the common range of inference steps. Such consistency suggests that the model is well-tuned to adapt to different conditions, making it effective for a wide range of applications. We also do exploration studies on the other hyper-parameters, such as batch size, the training epochs, and CFG values in Appendix Table 12. The studied optimal settings are the batch size with 64, the training epochs with 30, and the CFG value with 5.5. Moreover, we explore the influences of different amounts of training samples, shown in Appendix Table 17.

Ablation Studies. We conduct ablation studies about the architecture designs of NPNet in Table 4. The results show that both *singular value prediction* and *residual prediction* contribute to the final optimal results, while the *singular value prediction* component plays a more important role. We also empirically verify the effectiveness of data selection strategies in Appendix Tables 9 and 10.

4.3. Efficiency Analysis and Downstream Tasks

Efficiency Analysis. As a plug-and-play module, it is essential to discuss the memory consumption and inference latency of NPNet. Remarkably, NPNet achieves significant performance improvements even with fewer inference steps and reduced time costs in Fig. 5. Even when operating at the same number of inference steps in Appendix Table 11, our model introduces only a 0.4-second delay while synthesizing high-quality images, demonstrating its efficiency. Additionally, Appendix Fig. 15 shows its memory consumption is mere 500 MB, highlighting its resource-friendly design.

Our model not only delivers superior results but also exhibit significant application potential and practical value due to the impressive deployment efficiency.

Exploration of Downstream Task. We explored the potential of integrating NPNet with downstream tasks, specifically by combining it with ControlNet [58] for controlled image synthesis. As a plug-and-play module, our NPNet can be seamlessly incorporated into ControlNet. Visualization results in Appendix Fig. 20 demonstrate that this integration leads to the synthesis of more detailed and higher-quality images with higher semantic faithfulness, highlighting the effectiveness of our approach.

5. Conclusion

In this paper, we introduce a novel concept termed the *noise prompt*, which aims to transform random Gaussian noise into a golden noise by incorporating a small perturbation derived from the text prompt. Building upon this, we firstly formulate a *noise prompt learning* framework that systematically obtains “prompted” golden noise associated with a text prompt for diffusion models, by constructing a *noise prompt dataset* collection pipeline that incorporates HPSv2 to filter our data and designing several backbones for our *noise prompt models*. Our extensive experiments demonstrate the superiority of NPNet, which is plug-and-play, straightforward, and nearly time-efficient, while delivering significant performance improvements. We believe that the future application of NPNet will be broad and impactful, encompassing video, 3D content, and seamless deployment of AIGC products, thereby making a meaningful contribution to the community.

Acknowledgement

This work was supported by the Science and Technology Bureau of Nansha District Under Key Field Science and Technology Plan Program No. 2024ZD002. This work was supported by Guangdong Provincial Key Lab of Integrated Communication, Sensing and Computation for Ubiquitous Internet of Things (No.2023B1212010007).

References

- [1] Donghoon Ahn. Self-rectifying diffusion sampling with perturbed-attention guidance, 2024. 27
- [2] Donghoon Ahn, Jiwon Kang, Sanghyun Lee, Jaewon Min, Minjae Kim, Wooseok Jang, Hyoungwon Cho, Sayak Paul, SeonHwa Kim, Eunju Cha, Kyong Hwan Jin, and Seungryong Kim. A noise is worth diffusion guidance, 2024. 2
- [3] Shane Barratt and Rishi Sharma. A note on the inception score, 2018. 12
- [4] James Betker, Gabriel Goh, Li Jing, † TimBrooks, Jianfeng Wang, Linjie Li, † LongOuyang, † JuntangZhuang, † JoyceLee, † YufeiGuo, † WesamManassra, † PrafullaDhariwal, † CaseyChu, † YunxinJiao, and Aditya Ramesh. Improving image generation with better captions. 2
- [5] Hila Chefer, Yuval Alaluf, Yael Vinker, Lior Wolf, and Daniel Cohen-Or. Attend-and-excite: Attention-based semantic guidance for text-to-image diffusion models, 2023. 2, 14, 15
- [6] Hao Chen, Yujin Han, Diganta Misra, Xiang Li, Kai Hu, Difan Zou, Masashi Sugiyama, Jindong Wang, and Bhiksha Raj. Slight corruption in pre-training data makes better diffusion models, 2024. 13
- [7] Junsong Chen, Jincheng Yu, Chongjian Ge, Lewei Yao, Enze Xie, Yue Wu, Zhongdao Wang, James Kwok, Ping Luo, Huchuan Lu, and Zhenguo Li. Pixart- α : Fast training of diffusion transformer for photorealistic text-to-image synthesis, 2023. 2
- [8] Sherry X. Chen, Yaron Vaxman, Elad Ben Baruch, David Asulin, Aviad Moresheet, Kuo-Chin Lien, Misha Sra, and Pradeep Sen. Tino-edit: Timestep and noise optimization for robust diffusion-based image editing, 2024. 2
- [9] Hyungjin Chung, Jeongsol Kim, Geon Yeong Park, Hyelin Nam, and Jong Chul Ye. Cfg++: Manifold-constrained classifier free guidance for diffusion models, 2024. 27
- [10] Dhruva Ghosh, Hanna Hajishirzi, and Ludwig Schmidt. Geneval: An object-focused framework for evaluating text-to-image alignment, 2023. 5
- [11] Xiefan Guo, Jinlin Liu, Miaomiao Cui, Jiankai Li, Hongyu Yang, and Di Huang. Initno: Boosting text-to-image diffusion models via initial noise optimization, 2024. 2, 14, 15
- [12] Jack Hessel, Ari Holtzman, Maxwell Forbes, Ronan Le Bras, and Yejin Choi. Clipscore: A reference-free evaluation metric for image captioning, 2022. 2, 12
- [13] Martin Heusel, Hubert Ramsauer, Thomas Unterthiner, Bernhard Nessler, and Sepp Hochreiter. Gans trained by a two time-scale update rule converge to a local nash equilibrium, 2018. 7, 11
- [14] Jonathan Ho and Tim Salimans. Classifier-free diffusion guidance. In *Neural Information Processing Systems Workshop*, Virtual Event, 2021. NeurIPS. 3
- [15] Jonathan Ho, Ajay Jain, and Pieter Abbeel. Denoising diffusion probabilistic models. In *Neural Information Processing Systems*, pages 6840–6851, Virtual Event, 2020. NeurIPS. 19
- [16] Susung Hong. Smoothed energy guidance: Guiding diffusion models with reduced energy curvature of attention. In *The Thirty-eighth Annual Conference on Neural Information Processing Systems*, 2024. 15, 27
- [17] Susung Hong. Smoothed energy guidance: Guiding diffusion models with reduced energy curvature of attention, 2024. 15
- [18] Susung Hong, Gyuseong Lee, Wooseok Jang, and Seungryong Kim. Improving sample quality of diffusion models using self-attention guidance. In *Proceedings of the IEEE/CVF International Conference on Computer Vision*, pages 7462–7471, 2023. 27
- [19] Minghui Hu, Jianbin Zheng, Chuanxia Zheng, Chaoyue Wang, Dacheng Tao, and Tat-Jen Cham. One more step: A versatile plug-and-play module for rectifying diffusion schedule flaws and enhancing low-frequency controls, 2023. 13
- [20] Kaiyi Huang, Kaiyue Sun, Enze Xie, Zhenguo Li, and Xi-hui Liu. T2i-compbench: A comprehensive benchmark for open-world compositional text-to-image generation. *arXiv preprint arXiv:2307.06350*, 2023. 5
- [21] Jared Kaplan, Sam McCandlish, Tom Henighan, Tom B. Brown, Benjamin Chess, Rewon Child, Scott Gray, Alec Radford, Jeffrey Wu, and Dario Amodei. Scaling laws for neural language models, 2020. 22
- [22] Tero Karras, Miika Aittala, Timo Aila, and Samuli Laine. Elucidating the design space of diffusion-based generative models. *ArXiv*, abs/2206.00364, 2022. 19
- [23] Yuval Kirstain, Adam Polyak, Uriel Singer, Shahbuland Matiana, Joe Penna, and Omer Levy. Pick-a-pic: An open dataset of user preferences for text-to-image generation, 2023. 2, 5, 11
- [24] Kolors. Kolors: Effective training of diffusion model for photorealistic text-to-image synthesis. *arXiv preprint*, 2024. 2
- [25] Zhimin Li, Jianwei Zhang, Qin Lin, Jiangfeng Xiong, Yanxin Long, Xincheng Deng, and Yingfang Zhang. Hunyuan-dit: A powerful multi-resolution diffusion transformer with fine-grained chinese understanding, 2024. 2, 13
- [26] Shanchuan Lin, Anran Wang, and Xiao Yang. Sdxl-lightning: Progressive adversarial diffusion distillation, 2024. 7, 22
- [27] Tsung-Yi Lin, Michael Maire, Serge Belongie, Lubomir Bourdev, Ross Girshick, James Hays, Pietro Perona, Deva Ramanan, C. Lawrence Zitnick, and Piotr Dollár. Microsoft coco: Common objects in context, 2015. 11
- [28] Buhua Liu, Shitong Shao, Bao Li, Lichen Bai, Zhiqiang Xu, Haoyi Xiong, James Kwok, Sumi Helal, and Zeke Xie. Alignment of diffusion models: Fundamentals, challenges, and future, 2024. 2

- [29] Luping Liu, Yi Ren, Zhijie Lin, and Zhou Zhao. Pseudo numerical methods for diffusion models on manifolds, 2022. 19
- [30] Pengfei Liu, Weizhe Yuan, Jinlan Fu, Zhengbao Jiang, Hiroaki Hayashi, and Graham Neubig. Pre-train, prompt, and predict: A systematic survey of prompting methods in natural language processing, 2021. 3
- [31] Cheng Lu, Yuhao Zhou, Fan Bao, Jianfei Chen, Chongxuan Li, and Jun Zhu. Dpm-solver: A fast ode solver for diffusion probabilistic model sampling in around 10 steps. In *Neural Information Processing Systems*, New Orleans, LA, USA, 2022. NeurIPS. 19
- [32] Andreas Lugmayr, Martin Danelljan, Andres Romero, Fisher Yu, Radu Timofte, and Luc Van Gool. Repaint: Inpainting using denoising diffusion probabilistic models, 2022. 2, 13, 27
- [33] Simian Luo, Yiqin Tan, Longbo Huang, Jian Li, and Hang Zhao. Latent consistency models: Synthesizing high-resolution images with few-step inference, 2023. 7, 22
- [34] Chenlin Meng, Robin Rombach, Ruiqi Gao, Diederik P. Kingma, Stefano Ermon, Jonathan Ho, and Tim Salimans. On distillation of guided diffusion models, 2023. 4, 13
- [35] William Peebles and Saining Xie. Scalable diffusion models with transformers, 2023. 2
- [36] Pablo Pernias, Dominic Rampas, Mats L. Richter, Christopher J. Pal, and Marc Aubreville. Wuerstchen: An efficient architecture for large-scale text-to-image diffusion models, 2023. 2
- [37] Dustin Podell, Zion English, Kyle Lacey, Andreas Blattmann, Tim Dockhorn, Jonas Müller, Joe Penna, and Robin Rombach. Sdxl: Improving latent diffusion models for high-resolution image synthesis. In *The Twelfth International Conference on Learning Representations*, 2023. 2, 13
- [38] Zipeng Qi, Lichen Bai, Haoyi Xiong, and Zeke Xie. Not all noises are created equally: diffusion noise selection and optimization, 2024. 2, 14
- [39] Alec Radford, Jong Wook Kim, Chris Hallacy, Aditya Ramesh, Gabriel Goh, Sandhini Agarwal, Girish Sastry, Amanda Askell, Pamela Mishkin, Jack Clark, Gretchen Krueger, and Ilya Sutskever. Learning transferable visual models from natural language supervision, 2021. 12
- [40] Rafael Rafailov, Archit Sharma, Eric Mitchell, Stefano Ermon, Christopher D. Manning, and Chelsea Finn. Direct preference optimization: Your language model is secretly a reward model, 2024. 7
- [41] Robin Rombach, Andreas Blattmann, Dominik Lorenz, Patrick Esser, and Björn Ommer. High-resolution image synthesis with latent diffusion models. In *Proceedings of the IEEE/CVF Conference on Computer Vision and Pattern Recognition (CVPR)*, pages 10684–10695, 2022. 14, 15
- [42] Robin Rombach, Andreas Blattmann, Dominik Lorenz, Patrick Esser, and Björn Ommer. High-resolution image synthesis with latent diffusion models. In *Computer Vision and Pattern Recognition*, pages 10684–10695. IEEE, 2022. 2
- [43] Amirmojtaba Sabour, Sanja Fidler, and Karsten Kreis. Align your steps: Optimizing sampling schedules in diffusion models, 2024. 7
- [44] Seyedmorteza Sadat, Otmar Hilliges, and Romann M. Weber. Eliminating oversaturation and artifacts of high guidance scales in diffusion models, 2024. 27
- [45] Chitwan Saharia, William Chan, Saurabh Saxena, Lala Li, Jay Whang, Emily Denton, Seyed Kamyar Seyed Ghasemipour, Burcu Karagol Ayan, S. Sara Mahdavi, Rapha Gontijo Lopes, Tim Salimans, Jonathan Ho, David J Fleet, and Mohammad Norouzi. Photorealistic text-to-image diffusion models with deep language understanding, 2022. 5
- [46] Christoph Schuhmann. Improved aesthetic predictor. 2, 12
- [47] Chenyang Si, Ziqi Huang, Yuming Jiang, and Ziwei Liu. Freeu: Free lunch in diffusion u-net, 2023. 15, 27
- [48] Jiaming Song, Chenlin Meng, and Stefano Ermon. Denoising diffusion implicit models. In *International Conference on Learning Representations*, kigali, rwanda, 2023. OpenReview.net. 3, 19
- [49] GW Stewart. Matrix perturbation theory. *Computer Science and Scientific Computing/Academic Press, Inc*, 1990. 4
- [50] Michael Toker, Hadas Orgad, Mor Ventura, Dana Arad, and Yonatan Belinkov. Diffusion lens: Interpreting text encoders in text-to-image pipelines, 2024. 2
- [51] Fu-Yun Wang, Zhaoyang Huang, Alexander William Bergman, Dazhong Shen, Peng Gao, Michael Lingelbach, Keqiang Sun, Weikang Bian, Guanglu Song, Yu Liu, et al. Phased consistency model. *arXiv preprint arXiv:2405.18407*, 2024. 7, 22
- [52] Qiucheng Wu, Yujian Liu, Handong Zhao, Ajinkya Kale, Trung Bui, Tong Yu, Zhe Lin, Yang Zhang, and Shiyu Chang. Uncovering the disentanglement capability in text-to-image diffusion models, 2022. 2
- [53] Xiaoshi Wu, Yiming Hao, Keqiang Sun, Yixiong Chen, Feng Zhu, Rui Zhao, and Hongsheng Li. Human preference score v2: A solid benchmark for evaluating human preferences of text-to-image synthesis, 2023. 2, 5, 11
- [54] Zeke Xie, Qianyu Tang, Mingming Sun, and Ping Li. On the overlooked structure of stochastic gradients. In *Thirty-seventh Conference on Neural Information Processing Systems*, 2023. 4
- [55] Jiazheng Xu, Xiao Liu, Yuchen Wu, Yuxuan Tong, Qinkai Li, Ming Ding, Jie Tang, and Yuxiao Dong. Imagereward: Learning and evaluating human preferences for text-to-image generation, 2023. 2, 12
- [56] Katherine Xu, Lingzhi Zhang, and Jianbo Shi. Good seed makes a good crop: Discovering secret seeds in text-to-image diffusion models, 2024. 2
- [57] Hu Yu, Hao Luo, Fan Wang, and Feng Zhao. Uncovering the text embedding in text-to-image diffusion models, 2024. 2
- [58] Lvmin Zhang, Anyi Rao, and Maneesh Agrawala. Adding conditional control to text-to-image diffusion models, 2023. 8
- [59] Sixian Zhang, Bohan Wang, Junqiang Wu, Yan Li, Tingting Gao, Di Zhang, and Zhongyuan Wang. Learning multi-dimensional human preference for text-to-image generation. In *Proceedings of the IEEE/CVF Conference on Computer Vision and Pattern Recognition*, pages 8018–8027, 2024. 2, 12

A. Implementation Details

In this section, we present the benchmarks, evaluation metrics and the relevant contents we used in the main paper to facilitate a comprehensive understanding of our model’s performance. This overview will help contextualize our results and provide clarity on how we assessed the effectiveness of our approach.

A.1. Benchmarks

In our main paper, we conduct experiments across three popular text-to-image datasets.

Pick-a-Pic. Pick-a-Pic [23] is an open dataset designed to collect user preferences for images synthesized from text prompts. The dataset is gathered through a user-friendly web application that allows users to synthesize images and select their preferences. Each data sample includes a text prompt, two synthesized images, and a label indicating which the user prefers or a tie if there is no clear preference. The Pick-a-Pic dataset contains over 500,000 examples covering 35,000 unique prompts. Its advantage lies in the fact that the data comes from real users, reflecting their genuine preferences rather than relying on paid crowd workers

DrawBench. DrawBench is a newly introduced benchmark dataset designed for in-depth evaluation of text-to-image synthesis models. It contains 200 carefully crafted prompts categorized into 11 groups, testing the models’ abilities across various semantic attributes, including compositionality, quantity, spatial relationships, and handling complex text prompts. The design of DrawBench allows for a multidimensional assessment of model performance, helping researchers identify strengths and weaknesses in image synthesis. By comparing with other models, DrawBench provides a comprehensive evaluation tool for the text-to-image synthesis field, facilitating a deeper understanding of synthesis quality and image-text alignment.

HPD v2. The Human Preference Dataset v2 [53] is a large-scale, cleanly annotated dataset focused on user preferences for images synthesized from text prompts. It contains 798,090 binary preference choices involving 433,760 pairs of images, aiming to address the limitations of existing evaluation metrics that fail to accurately reflect human preferences. HPD v2 eliminates potential biases and provides a more comprehensive evaluation capability, with data sourced from multiple text-to-image synthesis models and real images.

GenEval. GenEval, an object-focused T2I benchmark to evaluate compositional image properties such as object co-occurrence, position, count, and color, contains 553

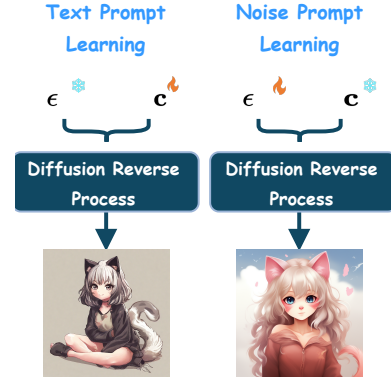


Figure 6. Paradigms of *text prompt learning* (left) and *noise prompt learning* (right).

prompts in total. This dataset plays a pivotal role in advancing research in text-to-image synthesis by providing a structured means to assess how well images align with the descriptive content of accompanying texts.

T2I-CompBench. T2I-CompBench is a comprehensive benchmark designed for evaluating the compositional capabilities of text-to-image (T2I) models, focusing on aspects such as object arrangement, relationships, and attributes within synthesized images. This benchmark consists of a diverse set of prompts that encompass various scenarios and contexts, facilitating a thorough assessment of how well T2I systems can interpret and visualize complex textual descriptions. By providing a structured framework for evaluation, T2I-CompBench significantly contributes to the advancement of research in T2I synthesis, offering insights into the strengths and limitations of current models in generating coherent and contextually accurate images.

For testing, we use these four popular T2I datasets, including the first 100 prompts subset from the Pick-a-Pic web application, 100 prompts from HPD v2 test set, all 200 prompts from DrawBench, all 553 prompts from GenEval and all test prompts in T2I-CompBench. The detailed information of the test sets is shown in Fig. 18.

A.2. Evaluation Metrics

In our main paper, we mainly include 6 evaluation metrics to validate the effectiveness of our NPNet.

PickScore. PickScore is a CLIP-based scoring function trained from the Pick-a-Pic dataset, which collects user preferences for synthesized images. It achieves superhuman performance when predicting user preferences. PickScore aligns well with human judgments, and together with Pick-a-Pic’s natural distribution prompts, enables much more relevant text-to-image model evaluation than evaluation standards, such as FID [13] over MS-COCO [27].



Figure 7. Visualization results about *re-denoise sampling*. *Re-denoise sampling* can help to inject semantic information of the text prompt into the original Gaussian noise.

HPSv2. Human Preference Score v2 (HPSv2) is an advanced preference prediction model by fine-tuning CLIP [39] on Human Preference Dataset v2 (HPD v2). This model aims to align text-to-image synthesis with human preferences by predicting the likelihood of a synthesized image being preferred by users, making it a reliable tool for evaluating the performance of text-to-image models across diverse image distribution.

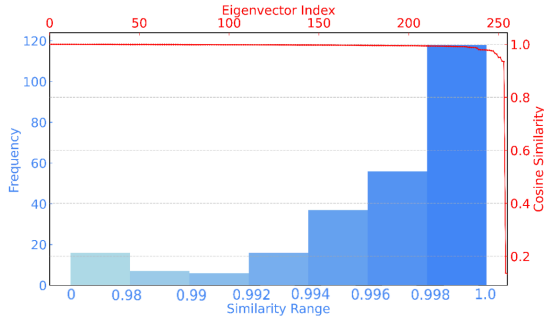


Figure 8. Visualization about the similarities between the singular vectors of \mathbf{x}_T and \mathbf{x}'_T . Note that we take the absolute values of the cosine similarity scores, and sort them reversely (the horizontal axis represents the indexes of the singular vectors).

AES. Aesthetic Score (AES) [46] are derived from a model trained on the top of CLIP embeddings with several extra multilayer perceptron (MLP) layers to reflect the visual appeal of images. This metric can be used to evaluate the aesthetic quality of synthesized images, providing insights into how well they align with human aesthetic preferences.

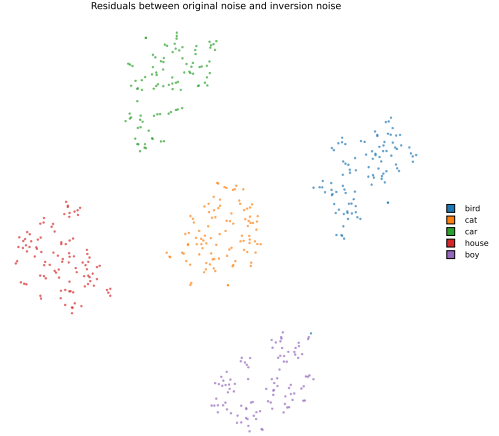


Figure 9. Using re-denoising sampling, we actively enhance the semantic information of the given prompt within the initial noise to enhance the semantic alignment of the generated images. This process is validated by the tight clustering of the residuals between the original noises and the inversion noises, each prompt with 100 noises, demonstrating the semantic information within the inversion noises.

ImageReward. ImageReward [55] is a human preference reward model specifically designed for evaluating text-to-image synthesis. It is trained on a large dataset of human comparisons, allowing it to effectively encode human preferences. The model assesses synthesized images based on various criteria, including alignment with the text prompt and overall aesthetic quality. ImageReward has been shown to outperform traditional metrics like Inception Score (IS) [3] and Fréchet Inception Distance (FID) in correlating with human judgments, making it a promising automatic evaluation metric for text-to-image synthesis.

CLIPScore. CLIPScore [12] leverages the capabilities of the CLIP model, which aligns images and text in a shared embedding space. By calculating the cosine similarity between the image and text embeddings, CLIPScore provides a measure of how well a synthesized image corresponds to its textual description. While CLIPScore is effective in assessing text-image alignment, it may not fully capture the nuances of human preferences, particularly in terms of aesthetic quality and detail².

MPS. Multi-dimensional Preference Score (MPS) [59], the first multi-dimensional preference scoring model for the evaluation of text-to-image models. The MPS intro-

²we follow <https://github.com/jmhessel/clipscore>

duces the preference condition module upon CLIP model to learn these diverse preferences. It is trained based on the Multi-dimensional Human Preference (MHP) Dataset, which comprises 918,315 human preference choices across four dimensions, including aesthetics, semantic alignment, detail quality and overall assessment on 607,541 images, providing a more comprehensive evaluation of synthesized images. MPS calculates the preference scores between two images, and the sum of the two preference scores equals 1.

A.3. T2I Diffusion Models

In the main paper, we totally use 3 T2I diffusion models, including StableDiffusion-xl (SDXL) [37], DreamShaper-xl-v2-turbo (DreamShaper), and Hunyuan-DiT (DiT) [25].

StableDiffusion-xl. StableDiffusion-xl (SDXL) is an advanced generative model, building upon the original Stable Diffusion architecture. This model leverages a three times larger UNet backbone, and utilizes a refinement model, which is used to improve the visual fidelity of samples synthesized by SDXL using a post-hoc image-to-image technique. SDXL is designed to synthesize high-resolution images from text prompts, demonstrating significant improvements in detail, coherence, and the ability to represent complex scenes compared to its predecessors.

DreamShaper-xl-v2-turbo. DreamShaper-xl-v2-turbo, a fine-tuned version on SDXL, is a text-to-image model designed for high-quality image synthesis, focusing on faster inference time and enhanced image synthesis capabilities. DreamShaper-xl-v2-turbo maintains the high-quality image output characteristic of its predecessor, while its turbo enhancement allows for quicker synthesis cycles. The overall style of the synthesized images leans towards fantasy, while it achieves a high level of authenticity when realism is required.

Hunyuan-DiT. Hunyuan-DiT is a text-to-image diffusion transformer with fine-grained understanding of both English and Chinese. With careful design of the model architecture, it can perform multi-turn multimodal dialogue with users to synthesized high-fidelity images, under the refinement of the Multimodal Large Language Model.

A.4. Model Architecture

Our NPNet consists of two branches, one is *singular value prediction*, and another is *residual prediction*.

For the *singular value prediction* branch, we process the decomposed SVD components through three parallel MLP branches: one for the orthogonal matrix U , one for V , and another for singular values s . Each branch contains two linear layers with ReLU activation. We combine them with a self-attention module to model global relationships,

followed by a residual MLP that adjusts the singular values while retaining their original characteristics through skip connections. The refined components are reconstructed via matrix operations to produce the output. The detail of the self-attention is illustrated in Fig. 11.

For the *residual prediction* branch, we employ a hybrid architecture combining a pretrained Swin-Tiny transformer with learnable up/down-sampling layers. The input is first upsampled to 224×224 resolution, projected to 3 channels via 1×1 convolution, then processed by the transformer’s feature extractor. Features are downsampled to the original resolution and projected back through another 1×1 convolution. An optional residual connection adds the input to the refined output.

A.5. Hyper-parameter Settings

Our method is straightforward and intuitive, and the parameter settings for the entire experiment are also very simple, with epoch 30, and batch size 64 for all experiments. During training, we surprise the observe that randomly assigning one prompt to the whole samples in one batch can yield a better model, where we speculate that such an operation could be considered as a strong regularizer as in Chen et al. [6]. We conduct experiments on three T2I diffusion models, including SDXL, DreamShaper-xl-v2-turbo and Hunyuan-DiT, with CFG ω_t 5.5, 3.5, and 5.0 respectively. The inverse CFG ω_w is 1.0 for all three models. To collect training data, the inference steps are 10, 4, and 10 for SDXL with DDIM inverse scheduler, Dreamshaper-xl-v2-turbo with DPMSolver inverse scheduler, and Hunyuan-DiT with DDIM inverse scheduler, respectively. The human preference model we use to filter the data is the HPSv2, and the filtering threshold k equals 0. Unless otherwise specified, all quantitative experiments and synthesized images in this paper are conducted and synthesize with inference steps 50, respectively. All experiments are conducted using $1 \times$ RTX 4090 GPUs, and all these noise pairs are collected with inference step 10 to construct NPDs.

B. Related Work

Synthesizing images that are precisely aligned with given text prompts remains a significant challenge for Text-to-Image (T2I) diffusion models. To deal with this problem, several works explore training-free improvement strategies, by optimizing the noises during the diffusion reverse process.

Lugmayr et al. [32] utilizes a pre-trained unconditional diffusion model as a generative prior and alters the reverse diffusion iterations based on the unmasked regions of the input image. Hu et al. [19] proposes to denoise one more step before the standard denoising process to eliminate the SNR noise discrepancy between training and inference. Meng et al. [34] observe that denoising the noise with inversion

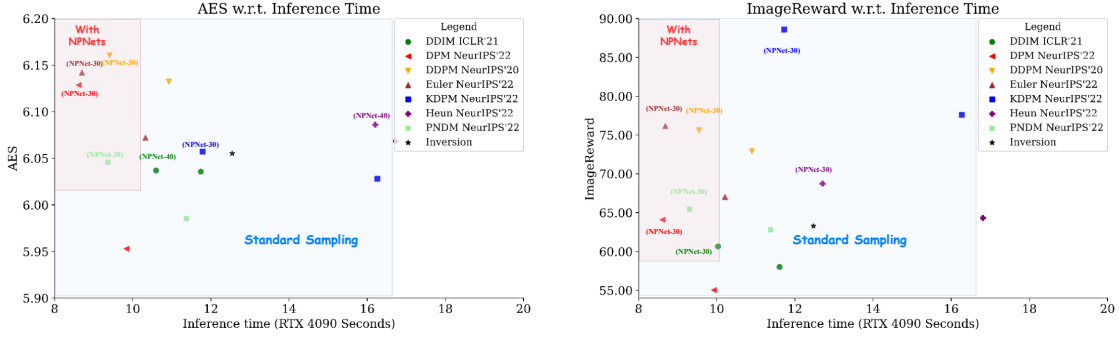


Figure 10. We evaluate our NPNet with 7 samplers on SDXL in Pick-a-Pic dataset, including both the deterministic sampler and stochastic sampler (with a default inference step 50). “NPNet-30” means the inference step is 30 with NPNet. The red area in the top left corner of the image represents the results of efficient high-performance methods, while the experimental results of NPNet are nearly in that same region. It highlights that NPNet is capable of synthesizing higher-quality images with fewer steps and consuming less time. Moreover, the results demonstrate the generalization ability of our NPNet across different samplers.

Table 6. Generalization on different diffusion models. We train our NPNet with NPD collected from SDXL. We apply it directly to DreamShaper-xl-v2-turbo on Pick-a-Pic dataset. Our results show promising performance, highlighting the model’s capability for cross-model generalization.

Inference Steps		PickScore (\uparrow)	HPSv2 (\uparrow)	AES (\uparrow)	ImageReward (\uparrow)
4	Standard	21.57	29.02	5.9172	53.12
	NPNet (ours)	21.62	29.20	5.9159	58.46
10	Standard	22.39	32.16	6.0296	96.67
	NPNet (ours)	22.41	32.24	6.0320	97.92
30	Standard	22.42	32.33	6.0116	98.97
	NPNet (ours)	22.44	32.48	6.0054	100.18
50	Standard	22.41	32.12	6.0161	98.09
	NPNet (ours)	22.47	32.25	6.0033	99.86

steps can generate better images compared with the original denoising process. Based on that, Qi et al. [38] aims to reduce the truncate errors during the denoising process, by increase the cosine similarity between the initial noise and the inversed noise in an end-to-end way. It introduces significant time costs, and the synthesized images may be over-rendered, making it difficult to use in practical scenarios.

Another research direction introduces extra modules to help optimize the noises during the reverse process. Chefer et al. [5] introduce the concept of Generative Semantic Nursing (GSN), and slightly shifts the noisy image at each timestep of the denoising process, where the semantic information from the text prompt is better considered. InitNO [11] consists of the initial latent space partitioning and the noise optimization pipeline, responsible for defining valid regions and steering noise navigation, respectively. Such methods are not universally applicable, we discuss this in Appendix C

Unlike previous approaches, we are the first to reframe

Table 7. Comparison results with InitNO on StableDiffusion-v1-4 [41] on Pick-a-Pic dataset. We directly apply NPNet trained for SDXL, and remove the embedding ϵ to StableDiffusion-v1-4.

	PickScore (\uparrow)	HPSv2 (\uparrow)	AES (\uparrow)	ImageReward (\uparrow)
Standard	19.17	19.49	5.4575	-122.73
InitNO	16.50	14.47	5.3116	-205.66
NPNet (ours)	19.25	19.54	5.5151	-95.89

this task as a learning problem. we directly learn to prompt the initial noise into the winning ticket noise to address this issue, by training a universal Noise prompt network (NPNet) with our noise prompt dataset (NPD). Our NPNet operates as a plug-and-play module, with very limited memory cost and negligible inference time cost, produce images with higher preference scores and better alignment with the input text prompts effectively.


```

class SVDNoiseUnet(nn.Module):
    def __init__(self,
        in_channels=in_channels,
        out_channels=out_channels,
        resolution=resolution): # resolution = size // 8
        super(SVDNoiseUnet, self).__init__()

        _in = int(resolution * in_channels // 2)
        _out = int(resolution * out_channels // 2)
        self.mlp1 = nn.Sequential(
            nn.Linear(_in, 64),
            nn.ReLU(inplace=True),
            nn.Linear(64, _out),
        )
        self.mlp2 = nn.Sequential(
            nn.Linear(_in, 64),
            nn.ReLU(inplace=True),
            nn.Linear(64, _out),
        )
        self.mlp3 = nn.Sequential(
            nn.Linear(_in, _out),
        )
        self.attention = Attention(_out)
        self.bn = nn.BatchNorm2d(_out)
        self.mlp4 = nn.Sequential(
            nn.Linear(_out, 1024),
            nn.ReLU(inplace=True),
            nn.Linear(1024, _out),
        )

    def forward(self, x, residual=False):
        b, c, h, w = x.shape
        x = einops.rearrange(x, "b (a c) h w -> b (a h) (c w)", a=2, c=2)
        U, s, V = torch.linalg.svd(x)
        U.T = U.permute(0, 2, 1)
        out = self.mlp1(U.T) + self.mlp2(V) + self.mlp3(s).unsqueeze(1)
        out = self.attention(out).mean(1)
        out = self.mlp4(out) + s
        pred = U @ torch.diag_embed(out) @ V
        return einops.rearrange(pred, "b (a h) (c w) -> b (a c) h w", a=2, c=2)

```

Figure 11. The implementation details of the self-attention module in *singular value prediction* branch.

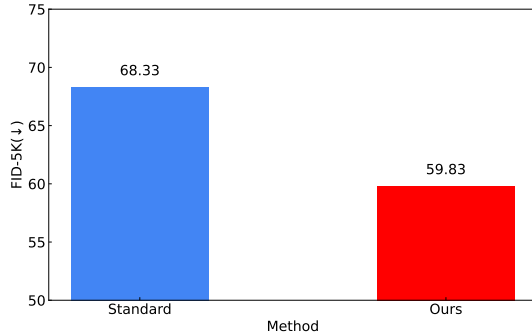


Figure 12. The FID comparison with 5000 images in class-conditional ImageNet with the resolution 512×512 . The results validate the effectiveness of our NPNet on improving the conventional image quality metric.

C. Discussion with the Previous Works

We previously mentioned that these methods [5, 11, 16, 17, 47], optimize the noise during the reverse process by incorporating additional modules. These methods have shown promising results in tasks involving compositional generalization. However, these methods often struggle to transfer to other datasets and models, making them not universally applicable. These approaches require the manual interest subject tokens, necessitating extensive test to identify the optimal tokens for a given sentence, which complicates their application across different datasets. Furthermore, modifying the model pipeline usually requires in-depth

code changes, making it difficult to achieve straightforward plug-and-play integration with other models. Moreover, these methods demand multiple rounds of noise optimization during the reverse process, resulting in significant time consumption.

In contrast, our approach addresses these challenges from multiple perspectives, offering a more flexible and universal solution. It is capable of cross-model and cross-dataset applications, provides plug-and-play functionality, and incurs minimal time overhead. We first follow the code in Guo et al. [11], and manually provide the subject tokens following Chefer et al. [5]. We conduct the experiments on StableDiffusion-v1-4 [41] on Pick-a-Pic dataset. Note that The authors did not provide the dataset or the necessary subject tokens for the algorithm, so we are limited to using our own dataset. Moreover, we had to manually select and trim the objects in the prompts. Additionally, the author’s code requires extensive modifications to the pipeline, making it difficult to adapt for use with other diffusion models. We directly apply the NPNet trained for SDXL to StableDiffusion-v1-4. The experimental results are shown in Table. 7, demonstrating the superiority of our NPNet. In addition, to prove that our method can be directly used in conjunction with other noise optimization methods, we directly use the NPNet trained on SDXL on these mainstream noise optimization methods, and the experimental results in Table. 20 and Fig. 19 prove that our NPNet can further improve the performance of other methods, which validates the generalizability of our NPNet.

D. Additional Experiment Results

D.1. Motivation

To the best of our knowledge, we are the first to propose the *noise prompt learning* framework, as illustrated in Fig. 6. In order to transform the random Gaussian noise into the golden noise, we utilize the *re-denoise sampling*, a straightforward method to boost the semantic faithfulness in the synthesized images, illustrated in Fig. 7, to obtain the noise pairs to construct our *noise prompt dataset*. Notably, in Fig. 9, we validate that re-denoising sampling can enhance the semantic information in the initial noise. When designing the architecture of *noise prompt network*, we discover the singular vectors between the source noise \mathbf{x}_T and target noise \mathbf{x}'_T exhibit remarkable similarity, albeit possibly in opposite directions, as shown in Fig. 8. Building upon this, we design the *singular value prediction* branch.

D.2. Exploration of Data Selection Strategies

Since the target noise collected through *re-denoise sampling* is not always of high quality, it is crucial to choose an appropriate method for data filtering. Effective selection ensures that only high-quality noise pairs are used, which

Table 8. We evaluate the effectiveness of our NPNet on T2I-CompBench benchmark. The results validate the effectiveness of our method.

Method	Attribute Binding			Object Relationship				Complex (↑)
	Color (↑)	Shape (↑)	Texture (↑)	2D-Spatial (↑)	3D-Spatial (↑)	Non-Spatial (↑)	numeracy (↑)	
Standard	0.5850	0.5028	0.5083	0.2097	0.3667	0.3113	0.5013	0.3130
Ours	0.5940	0.5094	0.5207	0.2146	0.3713	0.3151	0.5201	0.3174

is essential for training the NPNet, affecting the model’s performance and reliability. For this reason, we conduct experiments on the choice of human preference model to filter our data, shown in Appendix Table 9, here the filtering threshold $m = 0$. The results demonstrate that using HPSv2 ensures data diversity, allowing the filtered data to enhance the model’s performance effectively. This approach helps maintain a rich variety of training samples, which contributes to the model’s generalization ability and overall effectiveness.

We also explore the influence under difference filtering thresholds m , the results are shown in Appendix Table 10. Our findings reveal that while increasing the filtering threshold m can improve the quality of the training data, it also results in the exclusion of a substantial amount of data, ultimately diminishing the synthesizing diversity of the final NPNet.

D.3. Evaluate the Quality of Synthesized Images

To validate the quality of the synthesized images with our NPNet, we calculate the FID³ of 5000 images in class-conditional ImageNet with the resolution 512×512 on SDXL, shown in Appendix Fig. 12. Note that we just synthesize the “fish” class in the ImageNet dataset, whose directory ids are [n01440764, n01443537, n01484850, n01491361, n01494475, n01496331, n01498041]. The main fish class contains sub-class labels, including “tench”, “Tinca tinca”, “goldfish”, “Carassius auratus”, “great white shark”, “white shark”, “man-eater”, “man-eating shark”, “Carcharodon carcharias”, “tiger shark”, “Galeocerdo cuvieri”, “hammerhead”, “hammerhead shark”, “electric ray”, “crampfish”, “numbfish”, “torpedo”, “stingray”. Each time, we randomly choose one prompt with postfix “a class in ImageNet”, in order to synthesize ImageNet-like images. The results reveal that with our NPNet, the T2I diffusion models can synthesize images with higher quality than the standard ones.

D.4. Evaluate the probability density of synthesized images with NPNet

We visualize image distributions before and after NPNet by generating 50 images under identical conditions, using ImageNet images (1 class) as ground truth and text-to-im-

age SDXL for generation in Fig. 13. The experimental results show the use of NPNet, which enables the generated images to more closely resemble the real distribution, and more inclined to high-density regions.

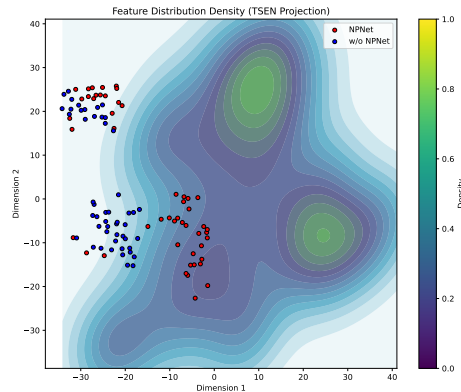


Figure 13. We visualize image distributions before and after NPNet by generating 50 images under identical conditions, using ImageNet images (1 class) as ground truth and text-to-image SDXL for generation. While text-to-image (v.s. class-conditioned) generation may induce distribution shifts, **NPNet shifts generation toward high-density regions.**

D.5. Generalization and Robustness

In this subsection, we provide more experiments to validate the generalization ability and robustness of our NPNet.

Generalization to Models, Datasets and Inference Steps.

In Appendix Table 6, we directly apply the NPNet for SDXL to DreamShaper-xl-v2-turbo without fine-tuning on the corresponding data samples. Even so, our NPNet achieves nearly the best performance across arbitrary inference steps, demonstrating the strong generalization capability of our model. Besides, we also present the winning rate of DreamShaper-xl-v2-turbo and Hunyuan-DiT across 3 different datasets, as presented in Appendix Fig. 14. These experimental results indicate that our method has a high success rate in transforming random Gaussian noise into winning noise, highlighting the effectiveness of our approach.

³We follow the code in <https://github.com/GaParmar/clean-fid>

Table 9. To collect valuable samples, we explore the data selection with different human preference models on SDXL with inference steps 10 on Pick-a-Pic dataset. “Standard*” here means no human preference model is applied.

Method	Filter Rate	PickScore (\uparrow)	HPSv2 (\uparrow)	AES (\uparrow)	ImageReward (\uparrow)
Standard*	-	21.21	25.95	5.9608	40.47
PickScore	34.28%	21.23	25.90	5.9750	32.56
HPSv2	23.88%	21.24	26.01	5.9675	42.47
AES	47.62%	21.22	25.83	5.9636	43.23
ImageReward	35.02%	21.2139	25.70	5.9580	32.39
PickScore+HPSv2	41.93%	21.23	25.75	5.9514	38.59
PickScore+ImageReward	52.57%	21.14	25.97	5.9936	42.19
All	74.41%	21.21	25.95	5.9608	40.47

Table 10. Experiments on the HPSv2 filtering threshold. We conducted experiments on SDXL on Pick-a-Pic dataset to investigate the impact of adding a threshold during the filtering process, like $s_0 + m < s'_0$, where s_0 and s'_0 are the human preference scores of denoising images \mathbf{x}_0 and \mathbf{x}'_0 .

Threshold	Filter Rate	PickScore (\uparrow)	HPSv2 (\uparrow)	AES (\uparrow)	ImageReward (\uparrow)
$m = 0$	23.88%	21.86	28.68	6.0540	66.21
$m = 0.005$	41.21%	21.78	28.79	6.0703	60.30
$m = 0.01$	50.19%	21.72	28.64	6.0766	61.60
$m = 0.02$	83.47%	21.82	28.78	6.0447	65.46

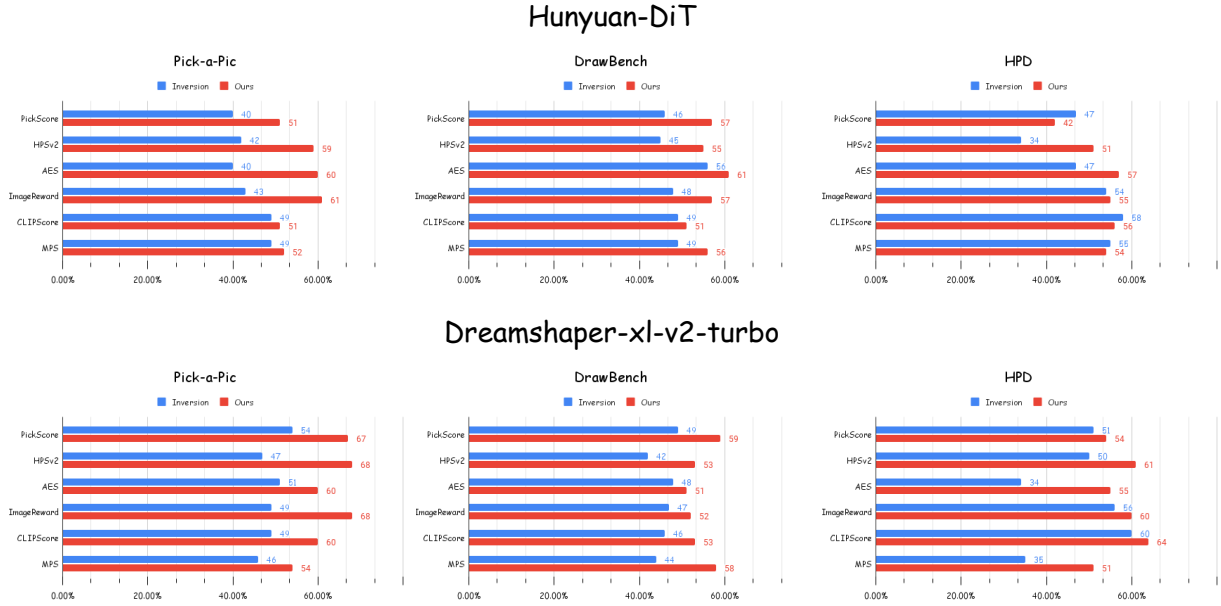


Figure 14. The winning rate comparison on DreamShaper-xl-v2-turbo and Hunyuan-DiT across 3 datasets, including Pick-a-Pic, DrawBench and HPD v2 (HPD) with inference steps 50. The results demonstrate the superiority of our NPNet.

Generalization to Random Seeds. As we mentioned in Sec. 3.2, the random seed range for the training set is $[0, 1024]$, while the random seed range for the test set is

$[0, 100]$. This discrepancy may lead to our NPNet potentially overfitting on specific random seeds. To evaluate the performance of our NPNet under arbitrary random seeds,

we artificially modified the seeds in the test set. The experimental results on the Pick-a-Pic dataset are presented in Appendix Table 19, demonstrating that our NPNet maintains strong performance across a variety of random seed conditions, making it suitable for diverse scenarios in real-world applications. The results demonstrate that our NPNet exhibits strong generalization capabilities across the out-of-distribution random seed ranges.

Robustness to Inference Steps and Hyper-parameters.

In Appendix Fig. 16, we conduct the experiments on DreamShaper-xl-v2-turbo and Hunyuan-DiT under various inference steps. The curve representing our method consistently remains at the top, demonstrating that our model achieves the best performance across various inference steps, further validating the robustness of our approach. To further support our claims, we present the winning rate of SDXL, DreamShaper-xl-v2-turbo and Hunyuan-DiT under various inference in two different datasets, shown in Appendix Fig. 17. These promising results validate the effectiveness of our NPNet.

Robustness to Hyper-parameters. We also conduct the experiments on different hyper-parameter settings, including the CFG value, batch size and training epochs, shown in Appendix Table 12. It reveals that the optimal setting of these parameters are CFG 5.5, batch size 64, and training epoch 30. For all the experiments in the paper, we all use this setting. Moreover, we explore the influence of the number of training samples, shown in Appendix Table 17, we believe that a large dataset can ensure data diversity and improve the model’s robustness and generalization ability.

D.6. Efficiency Analysis and Ablation Studies

Efficiency Analysis. As a plug-and-play module, it raises concerns about potential increases in inference latency and memory consumption, which can significantly impact its practical value. In addition to Fig. 5 presented in the main paper, we also measure the time required to synthesize each image under the same inference step conditions, shown in Appendix Table 11. Our model achieves a significant improvement in image quality with only a 0.4-second inference delay. Additionally, as shown in Appendix Fig. 15, our model requires just 500 MB of extra memory. These factors highlight the lightweight and efficient nature of our model, underscoring its broad application potential.

Ablation Studies. We explore the influence of the text embedding term \mathbf{e} . Although in Appendix Table 15, the value of α is very small, the results in Appendix Table 16 still demonstrate the importance of this term. It can facilitate a refined adjustment of how much semantic information influences the model’s predictions, enabling the semantic

relevance between the text prompt and synthesized images, and the diversity of the synthesized images.

D.7. Experiments on Large-scale Dataset

To evaluate the effectiveness of our NPNet, we conduct the experiments on a large-scale dataset, GenEval, across different T2I models. The results are shown in Appendix Table 13 and Table 14. The all improved metrics reveal the superiority of our NPNet, suggesting that our NPNet can improve the compositional image properties of the synthesized images.

E. Theoretical Understanding of Re-denoise Sampling

In main paper Sec. 3.1, we utilize *re-denoise sampling* to produce noise pairs. we propose to utilize DDIM-Inversion(\cdot) to obtain the noise from the previous step. Specifically, the joint action of DDIM-Inversion and CFG can induce the initial noise to attach semantic information. The mechanism behind this method is that DDIM-Inversion(\cdot) injects semantic information by leveraging the guidance scale in classifier-free guidance (CFG) inconsistency:

Theorem E.1. *Given the initial Gaussian noise $\mathbf{x}_T \sim \mathcal{N}(0, \mathbf{I})$ and the operators DDIM-Inversion(\cdot) and DDIM(\cdot). Using re-denoise sampling, we can obtain that:*

$$\mathbf{x}'_T = \mathbf{x}_T + \frac{\alpha_T \sigma_{T-k} - \alpha_{T-k} \sigma_T}{\alpha_{T-k}} \left[(\omega_l - \omega_w) (\epsilon_\theta(\mathbf{x}_{T-\frac{k}{2}}, T - \frac{k}{2} | \mathbf{c}) - \epsilon_\theta(\mathbf{x}_{T-\frac{k}{2}}, T - \frac{k}{2} | \emptyset)) \right]. \quad (10)$$

where k stands for the DDIM sampling step, \mathbf{c} is the text prompt, and ω_l and ω_w are CFG at the timestep T and CFG at timestep $T-k$, respectively.

Proof. One step *re-denoise sampling* represents one additional step forward sampling and one step reverse sampling against the initial Gaussian noise, which can be denoted as

$$\mathbf{x}'_T = \text{DDIM-Inversion}(\text{DDIM}(\mathbf{x}_T)), \quad (11)$$

where DDIM-Inversion(\cdot) refers to the sampling algorithm in Eqn. 1 when \mathbf{x}_t and \mathbf{x}_{t-1} are interchanged. We can

Table 11. Experiments on different samplers *w.r.t.* inference time cost on SDXL. The NPNet trained on noise samples produced by the deterministic sampler DDIM, demonstrates impressive generalization to non-deterministic samplers, incurring only minimal additional time costs.

Methods		PickScore (\uparrow)	HPSv2 (\uparrow)	AES (\uparrow)	ImageReward (\uparrow)	Time Cost(second per image)
DDIMScheduler [48]	Standard	21.69	28.48	6.0373	58.01	11.69
	NPNet (ours)	21.86	28.68	6.0540	65.01	12.10
DPM SolverMultistepScheduler [31]	Standard	21.66	28.41	5.9513	55.01	9.84
	NPNet (ours)	21.72	28.81	5.9744	67.30	10.43
DDPMScheduler [15]	Standard	21.78	28.72	6.1353	72.91	10.86
	NPNet (ours)	21.91	29.24	6.1505	78.50	11.43
EulerAncestralDiscreteScheduler [22]	Standard	21.72	28.66	6.0740	67.01	10.28
	NPNet (ours)	21.84	28.96	6.0886	85.05	10.86
PNDMScheduler [29]	Standard	21.78	29.35	5.9809	62.81	11.40
	NPNet (ours)	21.81	29.74	6.0256	67.58	11.82
KDPM2AncestralDiscreteScheduler [22]	Standard	21.81	29.22	6.0382	77.59	16.25
	NPNet (ours)	21.93	29.62	6.0951	84.78	16.73
HeunDiscreteScheduler [22]	Standard	21.83	28.71	6.0705	64.33	16.74
	NPNet (ours)	21.86	28.98	6.0892	73.31	17.04

Table 12. Ablation studies of the hyper-parameters on SDXL on Pick-a-Pic dataset.

Hyper-parameters		PickScore (\uparrow)	HPSv2 (\uparrow)	AES (\uparrow)	ImageReward (\uparrow)
Epochs	5	21.77	28.62	6.0688	65.84
	10	21.76	28.67	6.0629	60.59
	15	21.69	28.62	6.0721	58.74
	30	21.86	28.68	6.054	65.01
Guidance Scale	$\omega_1 = 1$	20.11	21.80	6.0601	-51.30
	$\omega_1 = 3$	21.53	27.28	6.0880	44.49
	$\omega_1 = 5.5$	21.86	28.68	6.0540	65.01
	$\omega_1 = 7$	21.81	29.12	6.0529	70.31
Batch Size	$bs = 16$	21.76	28.74	6.0677	60.80
	$bs = 32$	21.68	28.68	6.0483	65.47
	$bs = 64$	21.86	28.68	6.0540	65.01

Table 13. We evaluate the effectiveness of our NPNet on larger T2I benchmark, GenEval. The results validate the superiority of our method.

Model		PickScore (\uparrow)	HPSv2 (\uparrow)	AES (\uparrow)	ImageReward (\uparrow)
SDXL	Standard	22.58	28.00	5.4291	55.44
	Inversion	22.64	28.24	5.4266	58.37
	NPNet(ours)	22.73	28.41	5.4506	65.56
DreamShaper-xl-v2-turbo	Standard	23.51	31.20	5.5234	97.52
	Inversion	23.47	30.85	5.5157	95.91
	NPNet(ours)	23.59	31.24	5.5577	100.06
Hunyuan-DiT	Standard	23.15	30.46	5.6233	111.73
	Inversion	23.16	30.63	5.6210	111.98
	NPNet(ours)	23.15	30.69	5.7040	115.57

Table 14. We evaluate the effectiveness of our NPNet on Genval benchmark.

	Single (\uparrow)	Two (\uparrow)	Counting (\uparrow)	Colors (\uparrow)	Positions (\uparrow)	Color Attribution (\uparrow)	Overall (\uparrow)
Standard	97.50	63.64	36.25	85.11	8.00	19.00	51.58
NPNet (ours)	98.75	67.68	37.50	82.98	13.00	21.00	53.49

rewrite it in forms of linear transformation:

$$\begin{aligned}
\mathbf{x}'_T &= \alpha_T \left(\frac{\mathbf{x}_{T-k} - \sigma_{T-k} \epsilon_\theta(\mathbf{x}_{T-k}, T-k)}{\alpha_{T-k}} \right) + \sigma_T \epsilon_\theta(\mathbf{x}_{T-k}, T-k) \\
\mathbf{x}'_T &= \alpha_T \\
&\quad \left(\frac{\left(\alpha_{T-k} \left(\frac{\mathbf{x}_T - \sigma_T \epsilon_\theta(\mathbf{x}_T, T)}{\alpha_T} \right) + \sigma_{T-k} \epsilon_\theta(\mathbf{x}_T, T) - \sigma_{T-k} \epsilon_\theta(\mathbf{x}_{T-k}, T-k) \right)}{\alpha_{T-k}} \right) \\
&\quad + \sigma_T \epsilon_\theta(\mathbf{x}_{T-k}, T-k) \\
\mathbf{x}'_T &= \mathbf{x}_T - \sigma_T \epsilon_\theta(\mathbf{x}_T, T) + \frac{\alpha_T \sigma_{T-k}}{\alpha_{T-k}} \epsilon_\theta(\mathbf{x}_T, T) - \frac{\alpha_T \sigma_{T-k}}{\alpha_{T-k}} \epsilon_\theta(\mathbf{x}_{T-k}, T-k) \\
&\quad + \sigma_T \epsilon_\theta(\mathbf{x}_{T-k}, T-k) \\
\mathbf{x}'_T &= \mathbf{x}_T + \frac{\alpha_T \sigma_{T-k} - \alpha_{T-k} \sigma_T}{\alpha_{T-k}} [\epsilon_\theta(\mathbf{x}_T, T) - \epsilon_\theta(\mathbf{x}_{T-k}, T-k)], \tag{12}
\end{aligned}$$

where k stands for the DDIM sampling step. Substitute $\epsilon_\theta(\mathbf{x}_t, t) = (\omega + 1)\epsilon_\theta(\mathbf{x}_t, t|\mathbf{c}) - \omega\epsilon_\theta(\mathbf{x}_t, t|\emptyset)$ into Eq. 12, we can obtain

$$\begin{aligned}
\mathbf{x}'_T &= \mathbf{x}_T + \frac{\alpha_T \sigma_{T-k} - \alpha_{T-k} \sigma_T}{\alpha_{T-k}} \left[(\omega_l + 1)\epsilon_\theta(\mathbf{x}_T, T|\mathbf{c}) - \omega_l \epsilon_\theta(\mathbf{x}_T, T|\emptyset) \right. \\
&\quad \left. - (\omega_w + 1)\epsilon_\theta(\mathbf{x}_{T-k}, T-k|\mathbf{c}) + \omega_w \epsilon_\theta(\mathbf{x}_{T-k}, T-k|\emptyset) \right]. \tag{13}
\end{aligned}$$

Where ω_l and ω_w refer to the classifier-free guidance scale at the timestep T and the classifier-free guidance scale at timestep $T - k$, respectively. \mathbf{c} stands for the text prompt (*i.e.*, condition). Consider the first-order Taylor expansion $\epsilon_\theta(\mathbf{x}_{T-k}, T-k|\mathbf{c}) = \epsilon_\theta(\mathbf{x}_{T-\frac{k}{2}}, T-\frac{k}{2}|\mathbf{c}) + \frac{\mathbf{x}_{T-k} - \mathbf{x}_{T-\frac{k}{2}}}{2} \frac{\partial \epsilon_\theta(\mathbf{x}_{T-\frac{k}{2}}, T-\frac{k}{2}|\mathbf{c})}{\partial \mathbf{x}_{T-\frac{k}{2}}} + \frac{k}{2} \frac{\partial \epsilon_\theta(\mathbf{x}_{T-\frac{k}{2}}, T-\frac{k}{2}|\mathbf{c})}{\partial T-\frac{k}{2}} + \mathcal{O}((\frac{k}{2})^2)$ and $\epsilon_\theta(\mathbf{x}_T, T|\mathbf{c}) = \epsilon_\theta(\mathbf{x}_{T-\frac{k}{2}}, T-\frac{k}{2}|\mathbf{c}) + \frac{\mathbf{x}_T - \mathbf{x}_{T-\frac{k}{2}}}{2} \frac{\partial \epsilon_\theta(\mathbf{x}_{T-\frac{k}{2}}, T-\frac{k}{2}|\mathbf{c})}{\partial \mathbf{x}_{T-\frac{k}{2}}} - \frac{k}{2} \frac{\partial \epsilon_\theta(\mathbf{x}_{T-\frac{k}{2}}, T-\frac{k}{2}|\mathbf{c})}{\partial T-\frac{k}{2}} + \mathcal{O}((\frac{k}{2})^2)$,

when \mathbf{x}_T satisfies the condition $\left\| \frac{\mathbf{x}_T - \mathbf{x}_{T-k}}{k} \right\| \leq L$, where $L < +\infty$, Eq. 13 can be transformed into:

$$\begin{aligned}
\mathbf{x}'_T &= \mathbf{x}_T + \frac{\alpha_T \sigma_{T-k} - \alpha_{T-k} \sigma_T}{\alpha_{T-k}} \left[(\omega_l - \omega_w)(\epsilon_\theta(\mathbf{x}_{T-\frac{k}{2}}, T-\frac{k}{2}|\mathbf{c}) \right. \\
&\quad \left. - \epsilon_\theta(\mathbf{x}_{T-\frac{k}{2}}, T-\frac{k}{2}|\emptyset)) \right]. \tag{14}
\end{aligned}$$

The proof is complete. \square

By using Eqn. 14, when there is a gap between ω_l and ω_w , *re-denoise sampline* can be considered as a technique to inject semantic information under the guidance of future timestep ($t = T - \frac{k}{2}$) CFG into the initial Gaussian noise.

F. Discussion

Limitations. Although our experimental results have demonstrated the superiority of our method, the limitations still exist. As a machine learning framework, our method also faces classic challenges from training data quality and model architecture design. First, noise prompt data quality sets the performance limit of our method. The data quality is heavily constrained by *re-denoise sampling* and data selection, but lack comprehensive understanding. For example, there exists the potential risk that the proposed data collection pipeline could introduce extra bias due to the AI-feedback-based selection. Second, the design of NPNet is still somewhat rudimentary. While ablation studies support each component of NPNet, it is highly possible that more elegant and efficient architectures may exist and work well for the novel noise prompt learning task. Optimizing model architectures for this task still lacks principled understanding and remain to be a challenge.

Future Directions. Our work has various interesting future directions. First, it will be highly interesting to investigate improved data collection methods in terms of both performance and trustworthiness. Second, we will design more streamlined structures rather than relying on a parallel approach with higher performance or higher efficiency. For example, we may directly utilize a pre-trained diffusion model to synthesize golden noise more precisely. Third, we will further analyze and improve the generalization of our method, particularly in the presence of out-of-distribution prompts or even beyond the scope of T2I tasks.

Table 15. The values of the two trainable parameters α and β .

Model	α	β
SDXL	1.00E-04	-0.0189
DreamShaper-xl-v2-turbo	7.00E-05	0.0432
Hunyuan-DiT	2.00E-04	0.0018

G. More Visualization Results

We present more visualization results on different dataset, different diffusion models and with different noise optimization methods on Fig. 22, 23, 24, 25, 26, 27, 28, 29, 31, 30, 32 and 33.

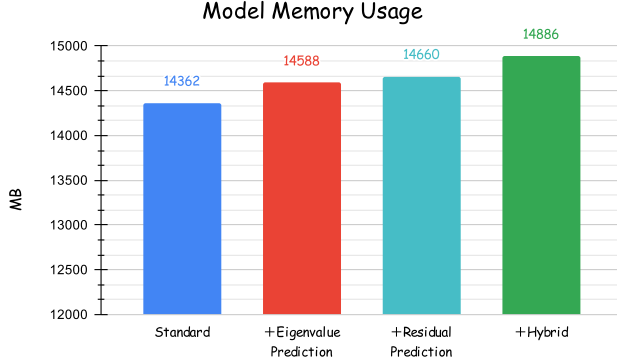


Figure 15. Our NPNet requires only about 500MB, illustrating the light-weight and efficiency of our model.

Table 16. We explore the influence of text embedding \mathbf{e} . The results reveal that text embedding \mathbf{e} is crucial in *noise prompt learning*, which aims to inject the semantic information into the noise.

Method	PickScore (\uparrow)	HPSv2 (\uparrow)	AES (\uparrow)	ImageReward (\uparrow)
NPNet w/o text embedding \mathbf{e}	21.72	28.70	6.0513	62.14
NPNet	21.86	28.68	6.0540	65.01

Algorithm 1: Noise Prompt Dataset Collection

- 1: **Input:** Timestep $t \in [0, \dots, T]$, random Gaussian noise \mathbf{x}_T , text prompt \mathbf{c} , DDIM operator $\mathbf{DDIM}(\cdot)$, DDIM inversion operator $\mathbf{DDIM-Inversion}(\cdot)$, human preference model Φ and filtering threshold m .
- 2: **Output:** Source noise \mathbf{x}_T , target noise \mathbf{x}'_T and text prompt \mathbf{c} .
- 3: Sample Gaussian noise x_T
- 4: # *re-denoise sampling*, see Sec. 3.1 in the main paper
- 5: $\mathbf{x}_{T-1} = \mathbf{DDIM}(\mathbf{x}_T)$
- 6: $\mathbf{x}'_T = \mathbf{DDIM-Inversion}(\mathbf{x}_{T-1})$
- 7: # *standard diffusion reverse process*
- 8: $\mathbf{x}_0 = \mathbf{DDIM}(\mathbf{x}_T)$
- 9: $\mathbf{x}'_0 = \mathbf{DDIM}(\mathbf{x}'_T)$
- 10: # *data filtering via the human preference model*, see Sec. 3.1
- 11: **if** $\Phi(\mathbf{x}_0, \mathbf{c}) + m < \Phi(\mathbf{x}'_0, \mathbf{c})$ **then**
- 12: store $(\mathbf{x}_T, \mathbf{x}'_T, \mathbf{c})$
- 13: **end if**

Algorithm 2: Noise Prompt Network Training

- 1: **Input:** Noise prompt dataset $\mathcal{D} := \{\mathbf{x}_{T_i}, \mathbf{x}'_{T_i}, \mathbf{c}_i\}_{i=1}^{|\mathcal{D}|}$, noise prompt model ϕ parameterized by singular value predictor $f(\cdot)$ and residual predictor $g(\cdot, \cdot)$, the frozen pre-trained text encoder $\mathcal{E}(\cdot)$ from diffusion model, normalization layer $\sigma(\cdot, \cdot)$, MSE loss function ℓ , and two trainable parameters α and β .
- 2: **Output:** The optimal noise prompt model ϕ^* trained on the training set \mathcal{D} .
- 3: # *singular value prediction*, see (6)
 $\tilde{\mathbf{x}}'_{T_i} = f(\mathbf{x}_{T_i})$
- 4: # *residual prediction*, see (7)
 $\hat{\mathbf{x}}_{T_i} = g(\mathbf{x}_{T_i}, \mathbf{c}_i)$
- 5: # see (9)
 $\mathbf{x}'_{T_{pred_i}} = \alpha \sigma(\mathbf{x}_{T_i}, \mathcal{E}(\mathbf{c}_i)) + \tilde{\mathbf{x}}'_{T_i} + \beta \hat{\mathbf{x}}_{T_i}$
- 6: $\mathcal{L}_i = \ell(\mathbf{x}'_{T_{pred_i}}, \mathbf{x}'_{T_i})$
- 7: update ϕ
- 8: **return** ϕ^*

Algorithm 3: Inference with Noise Prompt Network

- 1: **Input:** Text prompt \mathbf{c} , the trained noise prompt network $\phi^*(\cdot, \cdot)$ and the diffusion model $f(\cdot, \cdot)$.
- 2: **Output:** The golden clean image \mathbf{x}'_0 .
- 3: Sample Gaussian noise x_T
- 4: # get the golden noise
 $\mathbf{x}'_{T_{pred}} = \phi^*(\mathbf{x}_T, \mathbf{c})$
- 5: # standard inference pipeline
 $\mathbf{x}'_0 = f(\mathbf{x}'_{T_{pred}}, \mathbf{c})$
- 6: **return** \mathbf{x}'_0

Table 17. In order to explore the scaling law [21] in NPNet, we train our NPNet with different numbers of training samples on SDXL on Pick-a-Pic dataset.

Numbers of Training Samples	Method	PickScore (\uparrow)	HPSv2 (\uparrow)	AES (\uparrow)	ImageReward (\uparrow)	CLIPScore(%) (\uparrow)	MPS(%) (\uparrow)
3W	Standard	21.69	28.48	6.0373	58.01	82.04	-
	NPNet (ours)	21.82	28.78	6.0750	67.26	82.17	50.63
6W	NPNet (ours)	21.75	28.65	6.0392	64.56	81.98	51.60
10W	NPNet (ours)	21.86	28.68	6.0540	65.01	84.08	52.15

Table 18. We evaluate NPNet on few steps T2I diffusion models, like LCM [33], PCM [51] and SDXL-Lightning [26] on GenEval dataset. Here we use the NPNet from SDXL, and the results demonstrate NPNet can generalize well to different kinds of T2I diffusion models, boosting their performance directly.

Model		PickScore (\uparrow)	HPSv2 (\uparrow)	AES (\uparrow)	ImageReward (\uparrow)	CLIPScore (\uparrow)
SDXL-Lightning (4 steps)	Standard	22.85	29.12	5.6521	59.02	0.8093
	NPNet(ours)	23.03	29.71	5.7178	72.67	0.8150
LCM (4 steps)	Standard	22.30	26.52	5.4932	33.21	0.8050
	NPNet(ours)	22.38	26.83	5.5598	37.08	0.8123
PCM (8 steps)	Standard	22.05	26.98	5.5245	23.28	0.8031
	NPNet(ours)	22.22	27.59	5.5667	35.01	0.8175

Table 19. Random seed generalization experiments on SDXL with difference inference steps on Pick-a-Pic dataset. The random seeds of our training set range from [0, 1024], containing the random seeds of our test set. To explore the generalization ability of NPNet on out-of-distribution random seeds, we manually adjust the random seed range of the test set.

Inference Steps	Random Seed Range		PickScore (\uparrow)	HPSv2 (\uparrow)	AES (\uparrow)	ImageReward (\uparrow)
50	[0, 1024] (Original)	Standard	21.69	28.48	6.0373	58.01
		Inversion	21.71	28.57	6.0503	63.27
		NPNet (ours)	21.86	28.68	6.0540	65.01
	[2500, 3524]	Standard	21.63	28.57	5.9748	67.09
		Inversion	21.71	28.75	5.9875	70.92
		NPNet (ours)	21.81	29.02	5.9917	80.83
	[5000, 6024]	Standard	21.74	28.82	6.0534	78.02
		Inversion	21.78	29.04	6.0418	76.05
		NPNet (ours)	21.83	29.09	6.4220	79.84
	[7500, 7524]	Standard	21.70	29.12	6.0251	78.71
		Inversion	21.78	29.18	6.0541	82.69
		NPNet (ours)	21.81	29.02	6.0641	89.53
100	[0, 1024] (Original)	Standard	21.71	28.70	6.0041	61.76
		Inversion	21.72	28.70	6.0061	61.73
		NPNet (ours)	21.86	29.10	6.0761	74.57
	[2500, 3524]	Standard	21.69	28.73	5.9946	69.22
		Inversion	21.74	28.92	5.9863	71.86
		NPNet (ours)	21.81	29.04	5.9977	78.75
	[5000, 6024]	Standard	21.81	28.40	6.0489	79.57
		Inversion	21.85	28.66	6.0374	79.94
		NPNet (ours)	21.88	29.16	6.0576	83.87
	[7500, 7524]	Standard	21.73	28.67	6.0347	77.66
		Inversion	21.80	28.75	6.0600	82.33
		NPNet (ours)	21.86	29.12	6.0502	89.79

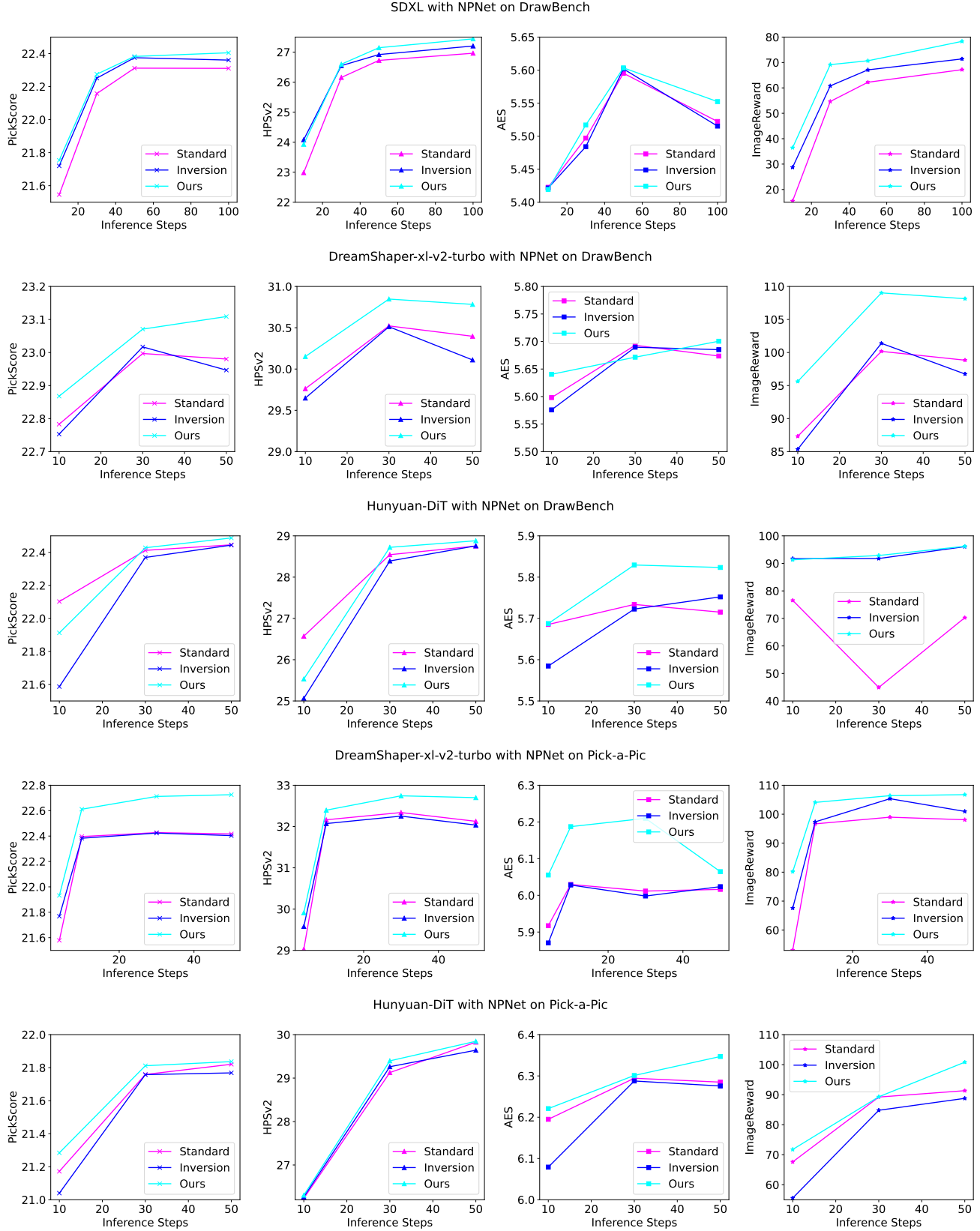


Figure 16. Visualization of performance w.r.t inference steps on SDXL, DreamShaper-xl-v2-turbo and Hunyuan-DiT on Pick-a-Pic dataset and DrawBench dataset. The results demonstrate the strong generalization ability of our NPNet.

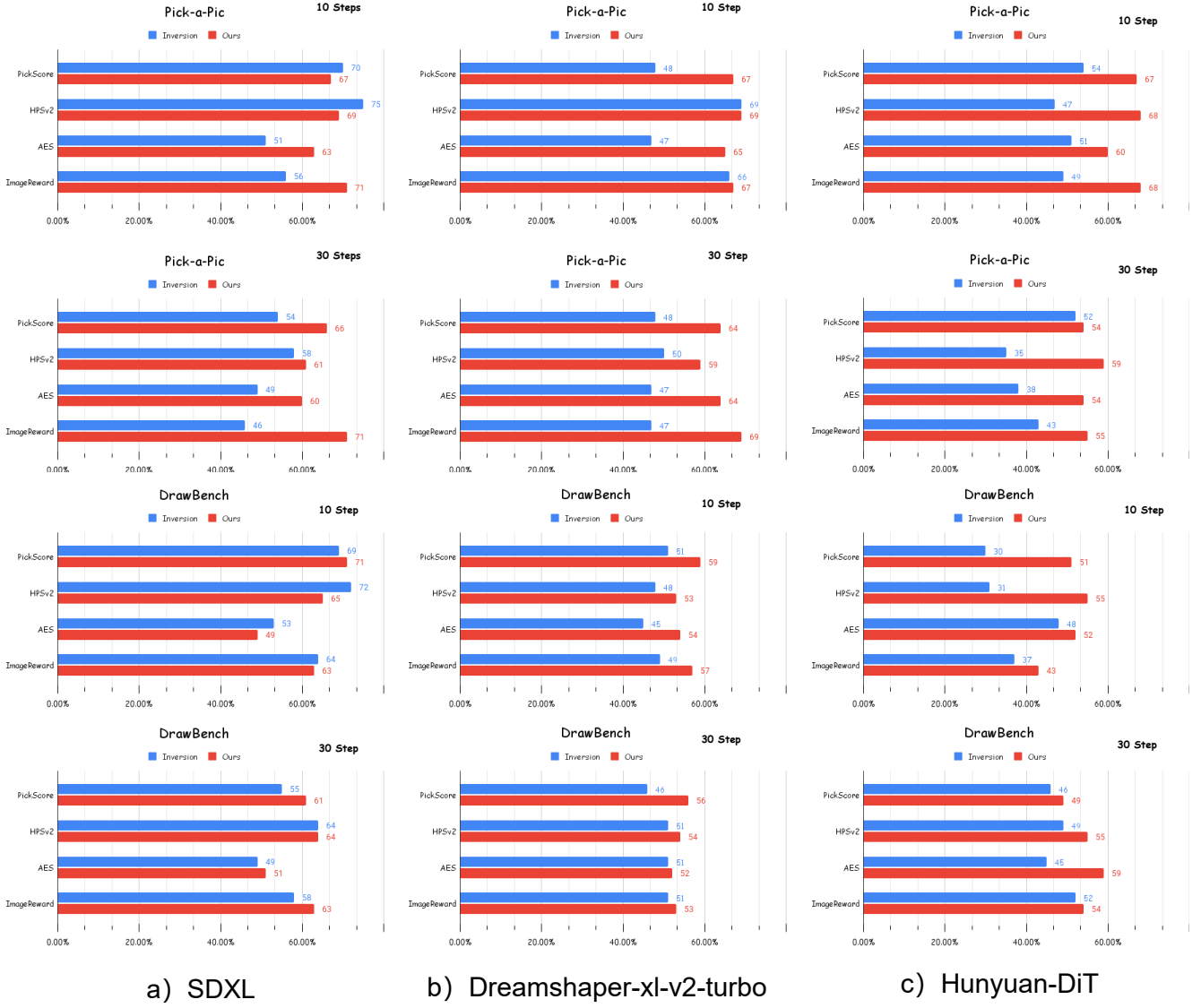


Figure 17. The winning rate comparison on SDXL, DreamShaper-xl-v2-turbo and Hunyuan-DiT across 2 datasets, including DrawBench and HPD v2 (HPD). The results reveal that our NPNet is more effective in transforming random Gaussian noise into golden noises in different inference steps across different datasets.

Pick-a-Pic

A curious cat exploring a haunted mansion.

A spanish water dog breed as arthur morgan from red dead redemption.

Movie Still of The Joker wielding a red Lightsaber, Darth Joker a sinister evil clown prince of crime, HD Photograph.

A closeup portrait of a playful maid, undercut hair, apron, amazing body, pronounced feminine feature, kitchen, , freckles, flirting with camera.

Art nouveau style, a crystal emperor moth with iridescent wings at the center of the universe with 7 Cosmic Rays emanating from it, futuristic, astrological, metaphysical, mystical, golden mean, HD 4K, sharp detail, photo-realistic.

Anime style. Girl at a wood table.

Ancient prayer figures pond sitter bouldartmoor carra, Christian Krohg, melancholia

Black and white 1905 year futuristic portrait of professional photographer with camera in hand in a desert sadly covered by mushrooms.

• • •

DrawBench

Three cats and three dogs sitting on the grass.

A real life photography of super mario, 8k Ultra HD.

An IT-guy trying to fix hardware of a PC tower is being tangled by the PC cables like Laokoon. Marble, copy after Hellenistic original from ca. 200 BC. Found in the Baths of Trajan, 1506.

New York Skyline with 'Deep Learning' written with fireworks on the sky.

A realistic photo of a Pomeranian dressed up like a 1980s professional wrestler with neon green and neon orange face paint and bright green wrestling tights with bright orange boots.

A pear cut into seven pieces arranged in a ring.

A triangular orange picture frame. An orange picture frame in the shape of a triangle.

An American multinational technology company that focuses on artificial intelligence, search engine, online advertising, cloud computing, computer software, quantum computing, e-commerce, and consumer electronics.

• • •

HPD v2

An anime man in flight uniform with hyper detailed digital artwork and an art style inspired by Klimt

A hand-drawn cute gnome holding a pumpkin in an autumn disguise.

Gnomes are playing music during Independence Day festivities in a forest near Lake George.

A small green dinosaur toy with orange spots standing on its hind legs and roaring with its mouth open.

A cute rainbow kitten with different colored eyes in the chibi-style of Studio Ghibli is featured on a postcard.

A slime monster.

A digital anime portrait of tatsumaki with green curly hair and green eyes wearing a jacket.

Portrait of young Jerry Lewis in comic style.

• • •

GenEval

A photo of a stop sign and a toaster.

A photo of a red train and a purple bear.

A photo of a purple tennis racket and a black sink.

A photo of a blue vase and a black banana.

A photo of a bear above a spoon.

A photo of a bed right of a frisbee.

A photo of a zebra below a computer keyboard.

photo of a wine glass right of a hot dog.

A photo of a potted plant and a backpack.

A photo of four computer keyboards.

• • •

Figure 18. Part of our test datasets. All of the training and test datasets will be released.



Figure 19. Winning rate of noise optimization methods on three different datasets, using SDXL. The results demonstrate that when NPNet is used in conjunction with other noise optimization methods, it can enhance the winning rate of existing approaches to some extent.

Table 20. We combine other popular noise optimization methods with our NPNet, evaluating on three different datasets on SDXL. The experimental results indicate that when NPNet is used alongside other methods, it significantly enhances their performance, further validating the effectiveness and generalizability of our approach.

Dataset	Method	PickScore (\uparrow)	HPSv2 (\uparrow)	AES (\uparrow)	ImageReward (\uparrow)	CLIPscore (\uparrow)
Pick-a-Pic	Standard	21.69	28.48	6.0373	58.01	0.8204
	Re-sampling [32]	21.77	28.63	5.9875	64.94	0.8327
	+ NPNet (ours)	21.90	29.29	6.1491	71.09	0.8386
	PAG [1]	21.64	29.45	6.2246	55.91	0.7966
	+ NPNet (ours)	21.70	29.80	6.2411	62.03	0.8079
	CFG++ [9]	21.67	29.54	6.1239	75.16	0.8322
	+ NPNet (ours)	21.82	29.84	6.1703	81.60	0.8374
	APG [44]	21.69	28.48	6.1472	65.86	0.8295
	+ NPNet (ours)	21.86	29.13	6.1629	76.50	0.8322
	FreeU [47]	21.39	29.12	6.2134	79.74	0.8094
	+ NPNet (ours)	21.42	29.44	6.2194	77.42	0.8059
	SAG [18]	21.70	29.42	6.1507	59.61	0.8162
	+ NPNet (ours)	21.79	29.63	6.1535	65.75	0.8193
	SEG [16]	21.47	29.23	6.2118	61.60	0.8060
	+ NPNet (ours)	21.60	29.72	6.2253	72.51	0.8077
DrawBench	Standard	22.31	26.72	5.5952	62.21	0.8077
	Re-sampling	22.30	26.96	5.5104	64.07	0.8106
	+ NPNet (ours)	22.47	27.55	5.6487	75.36	0.8136
	PAG	22.25	27.81	5.7082	67.25	0.7965
	+ NPNet (ours)	22.34	28.17	5.7646	72.10	0.7989
	CFG++	22.35	28.28	5.6720	81.69	0.8230
	+ NPNet (ours)	22.45	28.67	5.7035	86.40	0.8263
	APG	22.29	26.94	5.6180	70.15	0.8194
	+ NPNet (ours)	22.46	27.73	5.6445	81.30	0.8182
	FreeU	21.97	27.31	5.7379	63.18	0.7973
	+ NPNet (ours)	22.04	27.87	5.7464	77.53	0.7998
	SAG	22.30	27.64	5.6651	64.56	0.8144
	+ NPNet (ours)	22.37	27.98	5.6998	72.18	0.8104
	SEG	22.16	28.08	5.7867	64.37	0.7979
	+ NPNet (ours)	22.30	28.51	5.8093	74.12	0.7985
HPD	Standard	22.88	29.71	5.9985	96.63	0.8734
	Re-sampling	22.91	29.78	5.9948	97.39	0.8775
	+ NPNet (ours)	22.96	30.16	6.0098	98.34	0.8787
	PAG	22.80	30.54	6.1180	90.94	0.8536
	+ NPNet (ours)	22.92	30.97	6.1091	106.24	0.8584
	CFG++	23.03	30.94	6.0269	107.70	0.8875
	+ NPNet (ours)	23.08	31.07	6.0533	109.06	0.8920
	APG	22.94	29.64	6.0572	97.90	0.8836
	+ NPNet (ours)	23.06	30.40	6.0232	111.55	0.8945
	FreeU	22.72	30.52	6.0907	97.03	0.8580
	+ NPNet (ours)	22.73	30.83	6.1148	102.77	0.8631
	SAG	22.86	30.37	6.0680	93.62	0.8670
	+ NPNet (ours)	22.92	30.71	6.0177	97.20	0.8748
	SEG	22.74	30.47	6.0841	91.86	0.8569
	+ NPNet (ours)	22.80	30.74	6.1160	104.16	0.8591

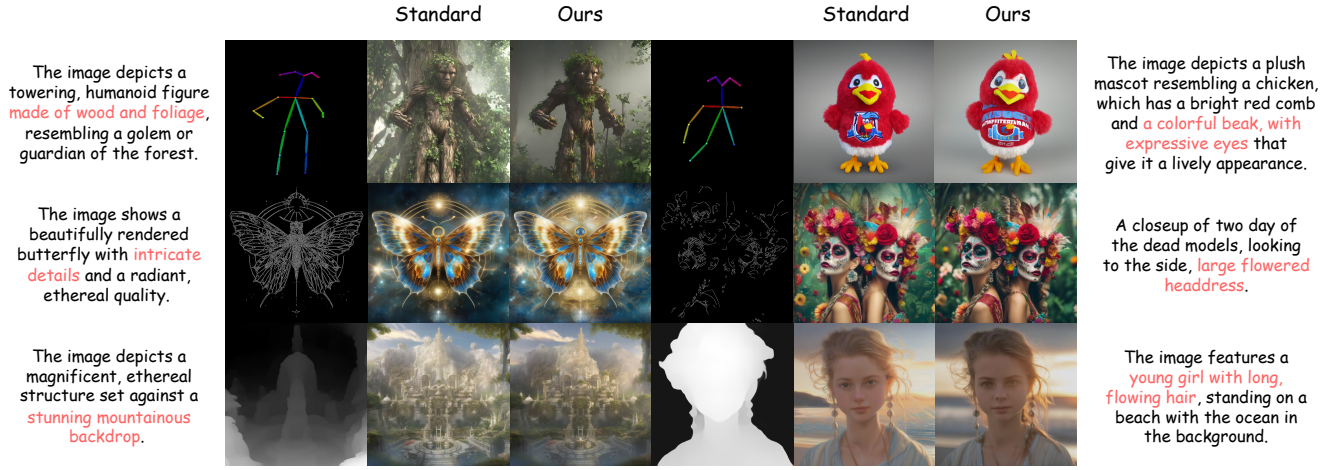


Figure 20. ControlNet visualization with our NPNet on SDXL, including conditions like openpose, canny and depth. *Middle* is the standard method, and *right* is our result. Our NPNet can be directly applied to the corresponding downstream tasks without requiring any modifications to the pipeline of the T2I diffusion model.

```

1  /* ---SDXL Inference Code--- */
2
3
4  # initialize the pipeline, scheduler and NPNet
5  pipe = StableDiffusionXLPipeline.from_pretrained(mode_id)
6  pipe.scheduler = DDIMScheduler.from_config(pipe.scheduler.config)
7  noise_model = NPNet()
8
9  # sample the initial noise
10 initial_noise = torch.randn(latent_shape)
11
12 # get the golden noise
13 prompt_embeds, _ = pipe.encode_prompt(prompt)
14 golden_noise = NPNet(prompt_embeds=prompt_embeds, initial_noise=initial_noise)
15
16 image = pipe(prompt=prompt, height=height, width=width, guidance_scale=guidance_scale,
17              num_inference_steps=num_steps, latents=golden_noise).images[0]

```

Figure 21. Example inference code with NPNet on SDXL. Our NPNet operates as a plug-and-play module, which can be easily implemented.

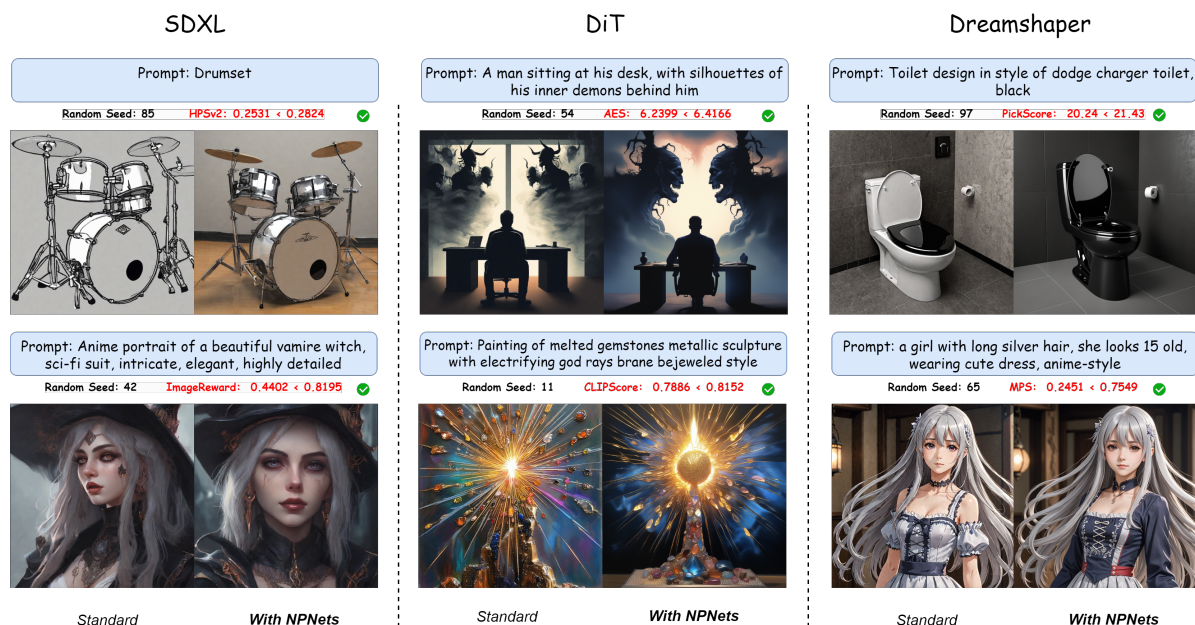


Figure 22. We visualized images synthesized by 3 different diffusion models and evaluated them using 6 human preference metrics. Images for each prompt are synthesized using the same random seed. These images with NPNet demonstrated a noticeable improvement in overall quality, aesthetic style, and semantic faithfulness, along with numerical improvements across all six metrics. More importantly, our NPNet is applicable to various diffusion models, showcasing strong generalization performance with broad application potential.

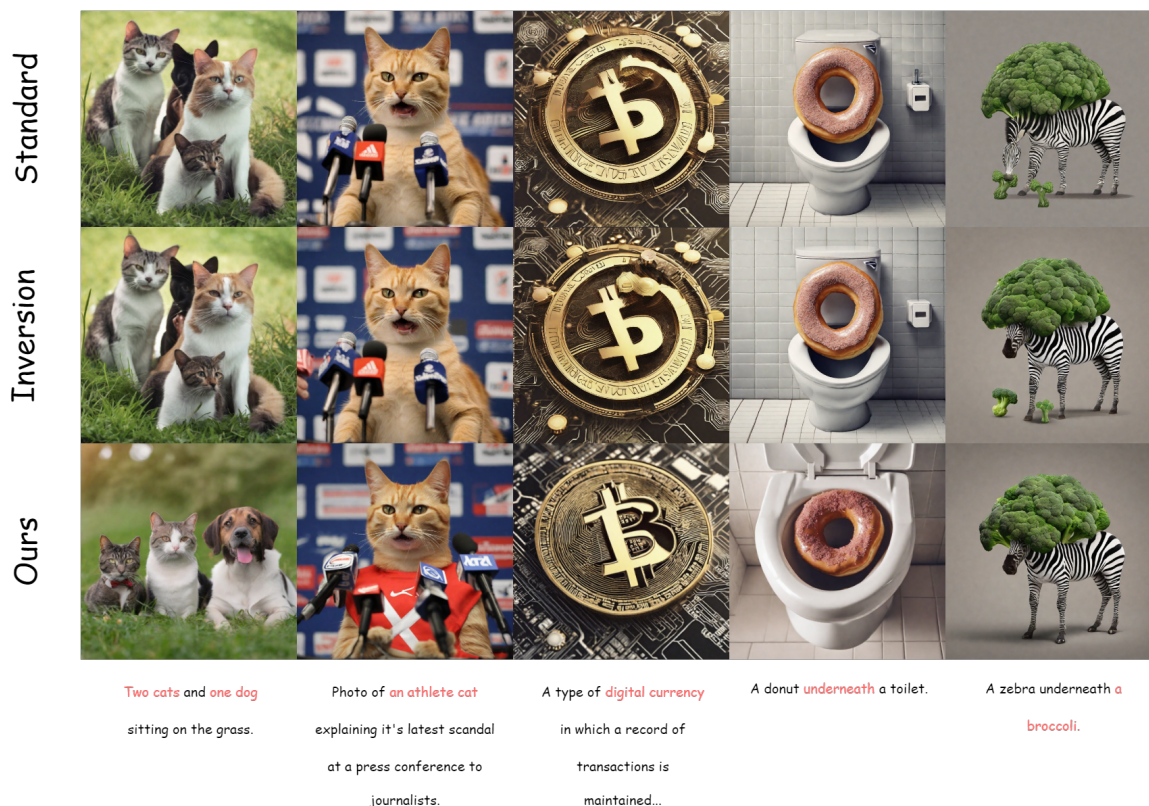


Figure 23. Visualization results about different methods on SDXL.



Figure 24. Qualitative comparison on LCM.

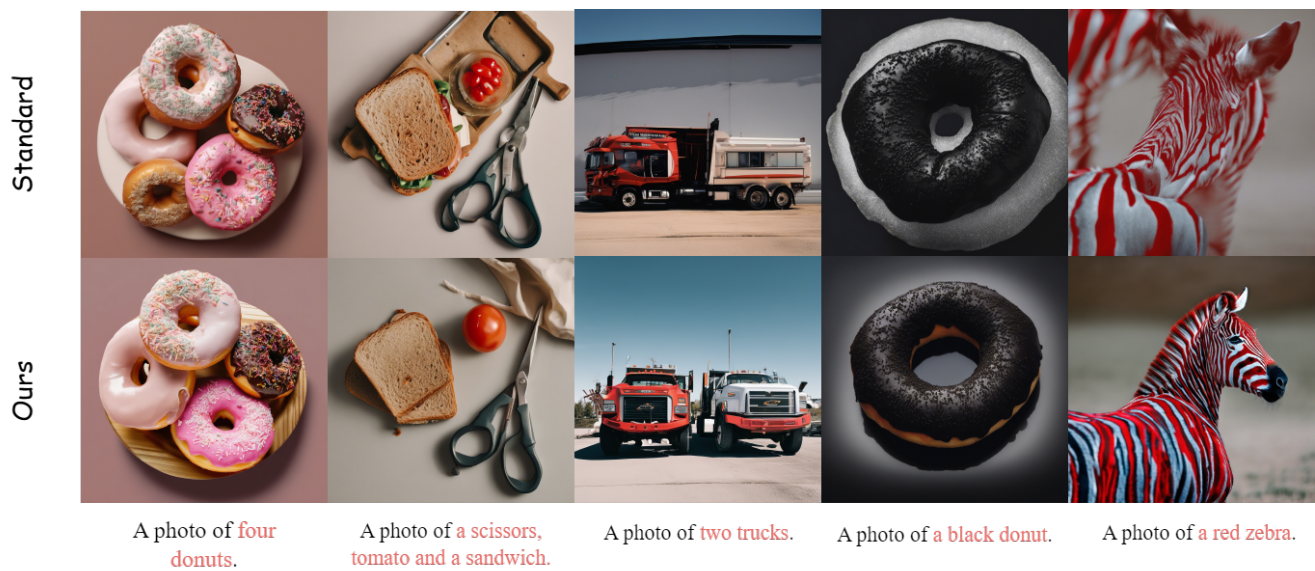


Figure 25. Qualitative comparison on PCM.



Figure 26. Qualitative comparison on SDXL-Lightning.



Figure 27. Qualitative comparison on Re-sampling.

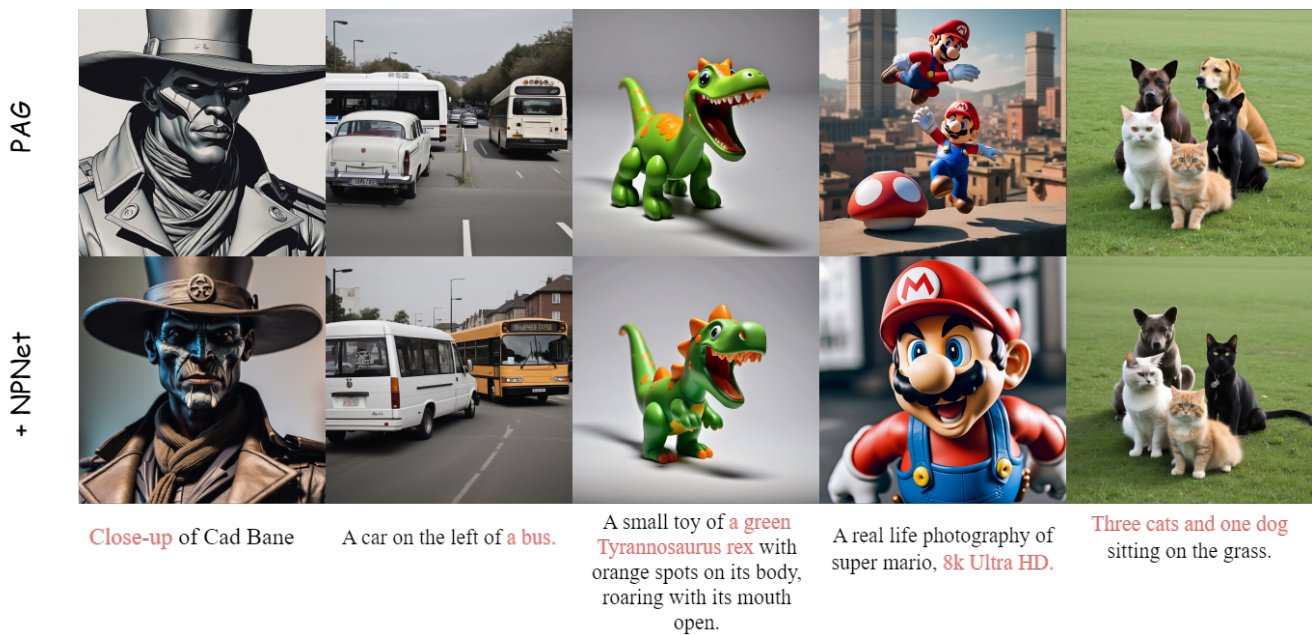


Figure 28. Qualitative comparison on PAG.

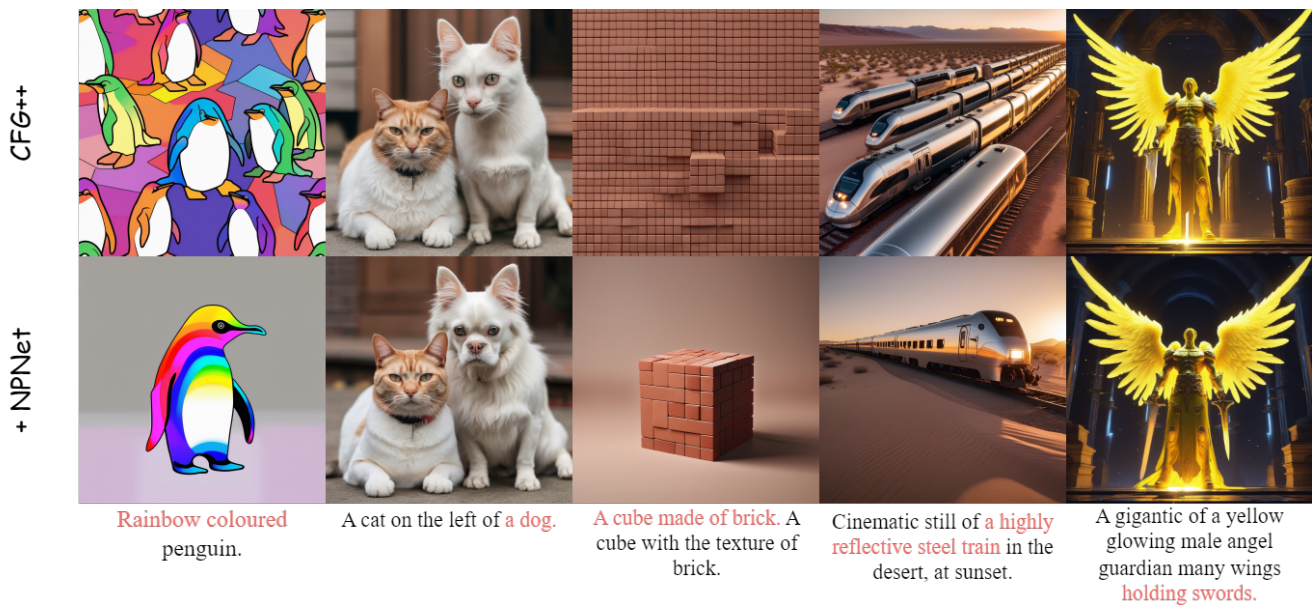


Figure 29. Qualitative comparison on CFG++.

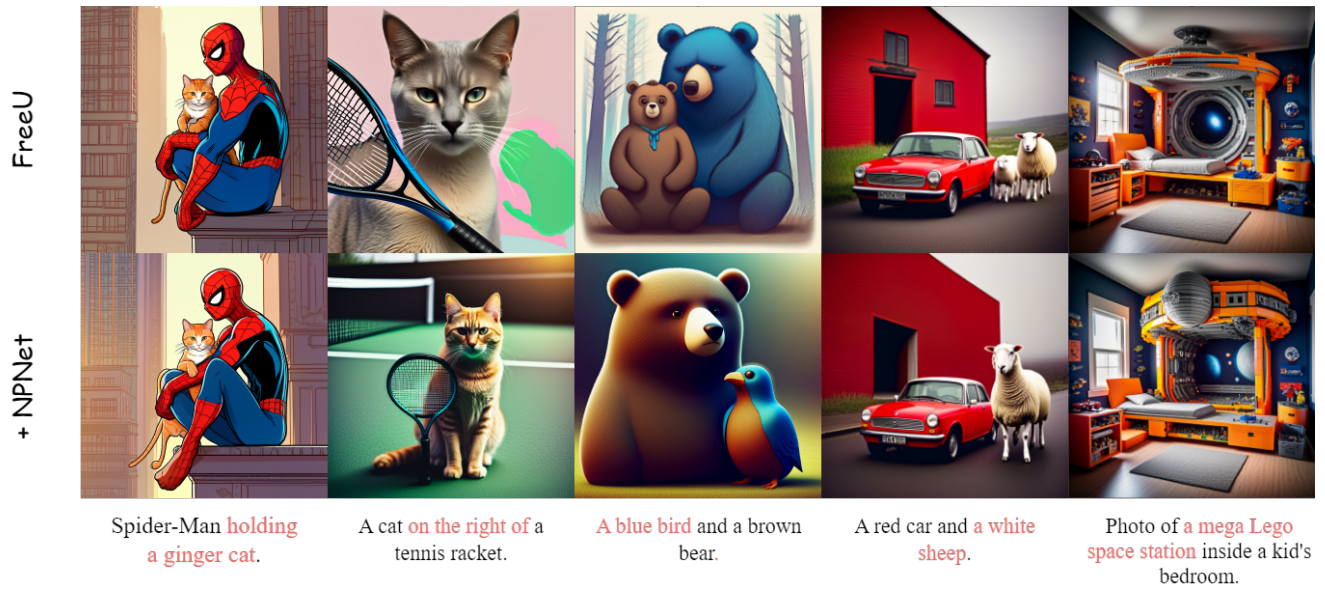


Figure 30. Qualitative comparison on FreeU.

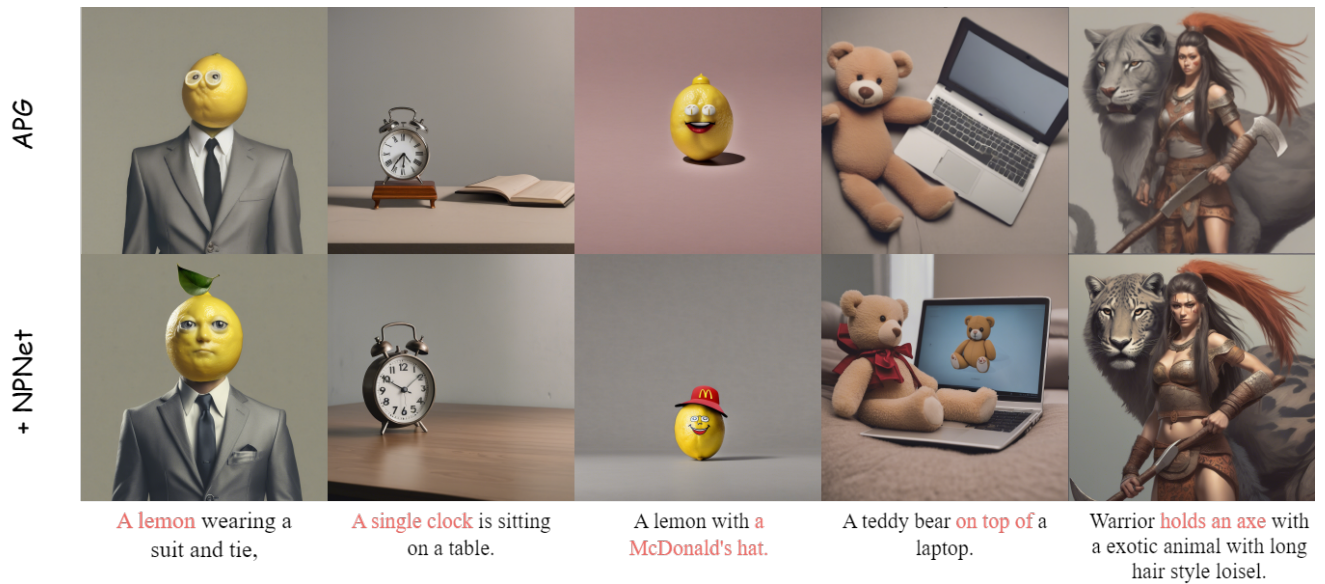


Figure 31. Qualitative comparison on APG.

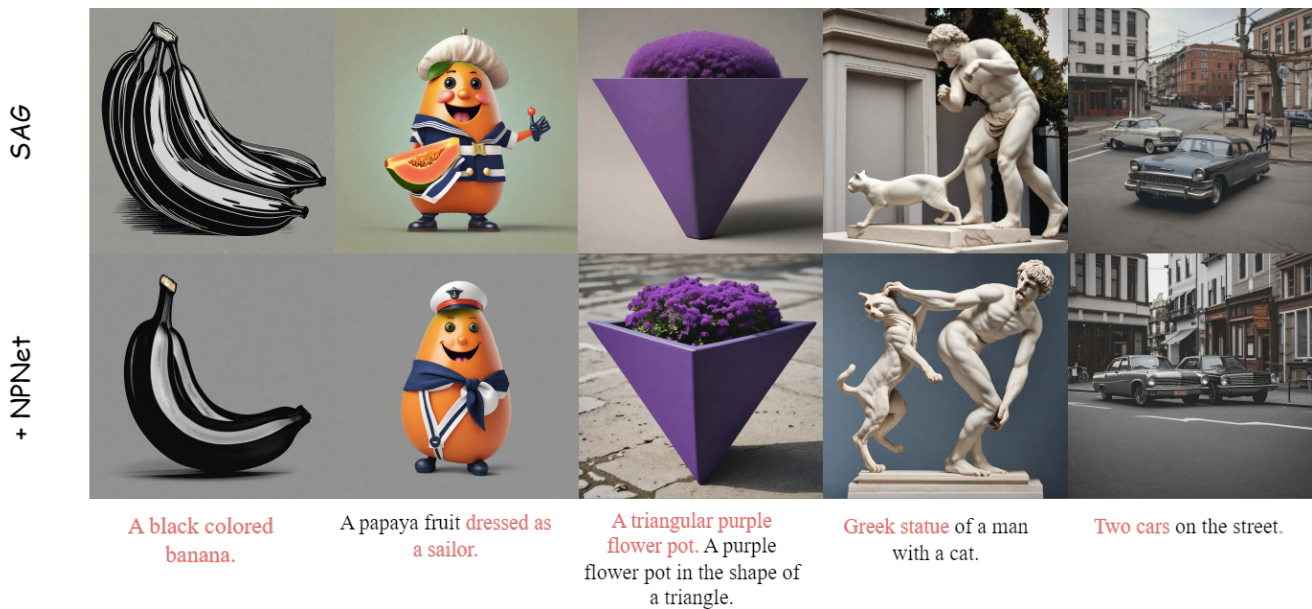


Figure 32. Qualitative comparison on SAG.



Figure 33. Qualitative comparison on SEG.